An Integrated Approach to Maneuver-Based Trajectory Prediction and Criticality Assessment in Arbitrary Road Environments

Matthias Schreier, Volker Willert, and Jürgen Adamy

***Abstract*—This paper describes an integrated Bayesian approach to maneuver-based trajectory prediction and criticality assessment that is not limited to specific driving situations. First, a distribution of high-level driving maneuvers is inferred for each vehicle in the traffic scene via Bayesian inference. For this purpose, the domain is modeled in a Bayesian network with both causal and diagnostic evidences and an additional trash maneuver class, which allows the detection of irrational driving behavior and the seamless application from highly structured to nonstructured environments. Subsequently, maneuver-based probabilistic trajectory prediction models are employed to predict each vehicle's configuration forward in time. Random elements in the designed models consider the uncertainty within the future driving maneuver execution of human drivers. Finally, the criticality time metric time-to-critical-collision-probability (TTCCP) is introduced and estimated via Monte Carlo simulations. The TTCCP is a generalization of the time-to-collision (TTC) in arbitrary uncertain multiobject driving environments and valid for longer prediction horizons. All uncertain predictions of all maneuvers of every vehicle are taken into account. Additionally, the criticality assessment considers arbitrarily shaped static environments, and it is shown how parametric free space (PFS) maps can advantageously be utilized for this purpose.**

***Index Terms*—Advanced Driver Assistance Systems (ADAS), criticality assessment, maneuver detection, parametric free space (PFS) map, time-to-collision (TTC), time-to-critical-collision-probability (TTCCP), trajectory prediction.**

I. Introduction and Motivation

FUTURE Advanced Driver Assistance Systems (ADAS) must not just react to the current state of the environment but anticipate the future evolution of the traffic scene to perform correct decisions, warnings, and interventions. Whereas this evolution can reasonably be predicted for a short time by just considering physical quantities such as estimated vehicle velocities or yaw rates, the evolution over several seconds is much stronger influenced by the intentions, motivations, and goals of all traffic participants within the specific driving environment. This raises the complexity for longer-term predictions considerably. Two major challenges exist in the design of long-term trajectory prediction and criticality assessment algorithms for active collision avoidance and warning systems. First, it is neither optimal to determine just a single future trajectory for each vehicle nor is it reasonable to predict every physically possible trajectory. In the first case, the one and only future hypothesis will most certainly not occur, whereas human drivers take different scene evolutions into account, see Fig. 1. In the second case, false warnings will be generated. For example, the reachable sets of two oncoming vehicles on different lanes overlap after a very short prediction horizon although this standard situation is usually uncritical and no warnings should be triggered.

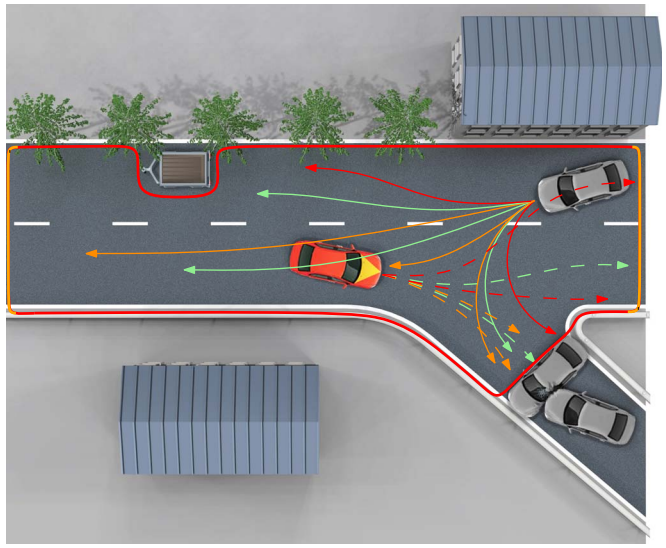

Fig. 1. Possible future scene evolutions in an exemplary driving scene. Both vehicles can turn, stay on their lane, or perform a lane change. Trajectories of possible future driving maneuver executions are shown in color—more probable ones in green, less probable ones in orange and red, respectively.

The second, less considered challenge is that the further one tries to predict into the future, the more assumptions have to be made, which tempts to model the average, sensible driver in a

Manuscript received December 19, 2014; revised April 25, 2015, July 24, 2015, and January 7, 2016; accepted January 23, 2016. Date of publication February 18, 2016; date of current version September 30, 2016. This work was supported by the Continental AG. The article is a revised and extended version of the paper entitled "Bayesian, Maneuver-Based, Long-Term Trajectory Prediction and Criticality Assessment for Driver Assistance Systems" presented at IEEE ITSC 2014, Qingdao, China, October 2014, and describes the complete, final system. Besides a visually more appealing presentation, the main extensions are the description of the probabilistic prediction models, the incorporation of parametric free space (PFS) maps, the generalization of the TTCCP calculation, and more in-depth explanations and results. The Associate Editor for this paper was D. Cao.

The authors are with the Institute of Automatic Control and Mechatronics, Control Methods and Robotics Laboratory, Technical University of Darmstadt, 64283 Darmstadt, Germany (e-mail: schreier@rtr.tu-darmstadt.de; vwillert@rtr.tu-darmstadt.de; jadamy@rtr.tu-darmstadt.de).

Color versions of one or more of the figures in this paper are available online at http://ieeexplore.ieee.org.

Digital Object Identifier 10.1109/TITS.2016.2522507

given traffic situation. As an extreme example, the prediction could be based upon the assumption that drivers obey traffic rules or follow the road flawlessly. Such assumptions are, however, inappropriate for active safety systems because especially actions that do not match the traffic rules and contradict with the standard situation evolution might become dangerous. Thus, all prediction methods that are solely based upon the average driver are not suitable for an emergency situation ADAS as exactly these situations are excluded by the prediction assumptions beforehand and therefore cannot be predicted at all.

Hence, the system i) must be sensitive to exceptional, rarely happening situations, ii) should not only consider physical quantities but also information about the drivers' intentions and the driving environment, and iii) take into account only a reasonable subset of possible future scene evolutions. As the drivers' intentions manifest in form of high-level driving maneuvers, it seems beneficial to first infer these more abstract hidden states. Our approach then connects the abstract, qualitative maneuver detection with the quantitative trajectory prediction domain with the ultimate goal to calculate a criticality metric suitable for arbitrary, uncertain driving environments and longer prediction time spans—the so-called Time-To-Critical-Collision-Probability (TTCCP).

II. Related Work

Long-term trajectory prediction methods can be classified into methods of pattern recognition in motion pattern databases [2], [3] and approaches fusing dynamic motion models with behavior and environment descriptions [4]–[10]. Besides the problem of generating, saving, and fitting large motion pattern data records, the first group has the disadvantage that only trajectories included in the database can be predicted. This makes them unsuitable for criticality assessment due to their inability to predict abnormal situations. Some representatives of the second group that additionally consider uncertainty are explained in the following.

The approaches of [5], [6] perform probabilistic trajectory predictions by employing path-planning algorithms from the viewpoint of each traffic participant to generate distributions over future motions of all vehicles. Different combinations of future system inputs are considered via Monte Carlo simulations, in which the stochastic inputs are restricted to specific, typical human driving behaviors and actions such as lane changes or overtaking—a similarity to our approach. They are, however, the result of goal functions, which model behaviors. No explicit maneuver detections are performed. The result is a probability of collision for the complete traffic scene as well as a so-called danger level display for each road position at each future time.

In [4], stochastic reachable sets of all other interacting traffic participants are determined assuming that they follow specific paths along a known road network with a certain accuracy. The ego vehicle's future path is considered available as the system is designed for autonomous vehicles with a known planned future trajectory and not for ADAS. The longitudinal dynamic motion models of other vehicles along their paths are abstracted into discrete Markov chains, the lateral positions are described by predefined, fixed distributions. The future actions "go straight" and "turn" are considered for the other vehicles. As their motions are constrained along road geometries and speed limits, an unintentional leaving of the road cannot be detected.

The approach of [7] allows longer-term criticality assessment in structured highway environments and focuses on the interaction of traffic participants. By updating a hand-designed prior intention distribution with results of the corresponding, fictive collision probabilities stemming from the execution of each intention, so-called interaction-aware maneuver probabilities are estimated. They are based on the postulation that drivers do not perform maneuvers with high collision risks as long as safer options are possible. This assumption, however, inevitably prevents the detection of specific dangerous situations such as colliding with a slower vehicle on the same lane if there is still a free adjacent lane for a possible lane change. Our approach, in contrast, predicts maneuvers only if physically measurable evidences indicate a maneuver.

Within the so-called PRIDE framework [10], estimation-theoretic short-term predictions are coupled with situation-based long-term prediction models. For the latter, cost functions are employed that describe the danger a driver would be exposed to if he executed a specific action sequence. A probability is associated with each predicted trajectory corresponding to an action. In a next step, each detected collision of a trajectory is used to adapt these probabilities retrospectively by assigning high costs to dangerous predictions. This procedure, however, excludes the prediction of critical trajectories due to their high costs, which makes it inappropriate for safety warning and intervention systems.

The approach described in [9] also employs behavior cost functions from which, after minimization, the future driver inputs of a (nearly) constant acceleration model are derived. A combination of longitudinal, lateral, interaction, and comfort cost functions is used. Deviations from a reference velocity, driving too close to the car in front, or abrupt braking and steering maneuvers are punished in the optimization process resulting in an adequate model for an average driver but cannot be used in this form for long-term criticality assessment.

Besides explicit trajectory prediction methods, numerous approaches reason about the future traffic scene on a more abstract level. The mathematical tools comprise deterministic and probabilistic state machines [11], static Bayesian networks [12]–[16], Dynamic Bayesian Networks (DBNs) [17], Hidden Markov Models (HMMs) [18], Dempster–Shafer theory [19], fuzzy theory [11], [12], special kinds of logics [20], or specific classifiers [21], [22]. Predictions with these models are normally performed on a more abstract, qualitative level, e.g., which driving maneuver a traffic participant is executing currently or in the near future, but not on the metric trajectory level relevant for quantitative criticality assessment. Exceptions, however, can be found in [8] and [23]. In the former, layered HMMs for maneuver detection are combined with spatio-temporal predictions, a similarity to our two-step approach, whereas the latter shows a particle filter-based system for simultaneous intention and trajectory estimation modeled within a DBN but not containing a criticality assessment part.

Within quantitative situation criticality assessment, deterministic Time-To-X (TTX) metrics, such as the Time-To-Collision (TTC) or the Time-To-React (TTR), are predominant [24], [25]. A recent extension [26] additionally considers uncertainty by calculating a probability distribution over TTCs via the Unscented Transform. In contrast to our approach, however, only uncertain state estimates are considered and not additional uncertainties in the drivers' behaviors. In [27], the authors calculate an evolution of collision probability over predicted time instants based on a weighted combination of a lane change maneuver model and a constant turn rate and acceleration model. A problem considering only individual, future time instants for criticality assessment is that possibly small collision probabilities within each future time step do not necessarily imply an uncritical situation. The criticality of the current situation can arise by an accumulation of criticality over a future time horizon—a topic treated further in Section III-C. In [28], continuous future risk indicator functions are introduced that incorporate uncertainty via critical event rates. This corresponds to modeling uncertainty not on trajectory level but on risk level, and a possible generalization of TTC is derived by considering distance-dependent event rates. The approach allows to generate warnings in near-collision scenarios as ours does. However, the risk is only "blurred" unimodally and symmetrically around the distance to closest encounter of two predicted vehicles in [28] and neither reflects the full multimodal uncertainties from different driving maneuvers nor nonlinear risk distortions. In contrast to the approaches mentioned this far, risk assessment can also be realized by comparing between what a driver is expected to do in a given traffic situation and the driver's actual intention. Expectations and intentions are estimated jointly in a Bayesian framework in [29], and risk is computed as the probability that expectation and intention do not match via particle filtering. This criticality metric, however, does not include any information *when* the situation is likely to become critical but only *whether* it becomes critical. Thus, it cannot be coupled with warning and intervention time thresholds in contrast to TTX metrics.

We connect a novel Bayesian network-based, qualitative maneuver detection with the quantitative, uncertain trajectory prediction domain to generate long-term predictions and use this as a basis for the introduced TTCCP criticality time metric that additionally considers arbitrary static environment configurations.

III. System Overview

The system is subdivided into three main parts: The maneuver detection, the prediction, and the criticality assessment part as shown in Fig. 2. In the maneuver detection part (blue), the current driving maneuver of every vehicle is estimated via Bayesian inference. For this purpose, a Bayesian network [30] is modeled and fed with measured vehicle and environment evidences, which are supposed to be available from preceding tracking, mapping, lane recognition, and localization systems. The inference result is a probability mass function (pmf) $p(M_{E,k})$ of the discrete maneuver random variable $M_{E,k}$ for the ego vehicle at each time step k as well as for the

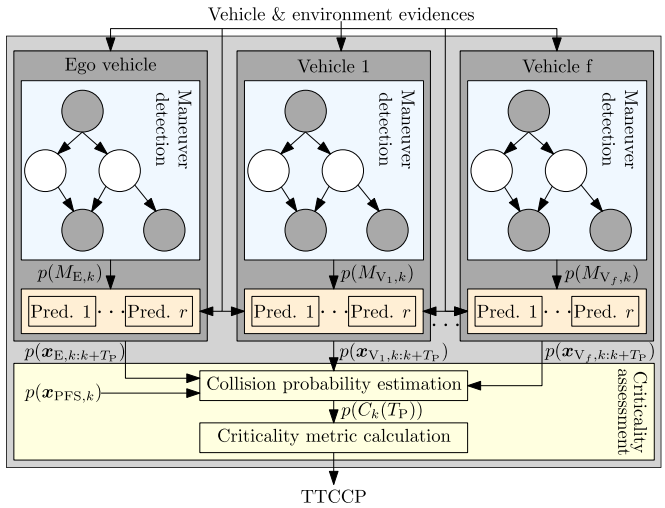

Fig. 2. System overview.

$i \in \{1, \ldots, f\}$ other vehicles $V_{i,k}$ within the observed traffic scene, $p(M_{V_i,k})$. In the prediction part (orange), maneuver-specific prediction models are employed to predict the configuration $\boldsymbol{x} = (x, y, \psi)^T$ of each vehicle forward in time within a common global coordinate system. The individual r prediction models are adapted to the current driving environment and uncertainties in the drivers' future maneuver realizations are taken into account by introducing uncertainties within these models. Therefore, even if we knew a driver is performing a specific maneuver for sure, the prediction model would nevertheless generate many possible trajectory realizations of this maneuver. The result of the prediction part is a joint probability distribution function (pdf) $p(\boldsymbol{x}_{k:k+T_P})$ of future configurations over the $T_P \in \mathbb{N}$ prediction time steps for each vehicle.[1] In the criticality assessment part (yellow), these individual joint distributions are used together with a Parametric Free Space (PFS) map-based representation of the static environment with pdf $p(\boldsymbol{x}_{\mathrm{PFS},k})$ to estimate the collision probability $p(C_k(T_P))$ of the event that the ego vehicle collides with at least one other vehicle or the static driving environment at least once within the prediction horizon $\{k{:}k + T_P\}$ via Monte Carlo simulation. Subsequently, the TTCCP criticality metric is calculated as the necessary prediction time until the probability of this collision event exceeds a certain value. It is therefore a time metric analogous to TTC, which, however, takes all possible future traffic scene evolutions into account. In the following, the three parts are explained in detail.

A. Maneuver Detection

The Bayesian network for maneuver detection is modeled with the application criticality assessment in mind and therefore needs to allow the detection of exceptional, non-standard situations. This can hardly be accomplished by modeling a single, complex network that takes interactions between all traffic participants into account. This approach would inevitably lead to the design of average traffic situations, thus preventing

[1]The sequence $k, k+1, \ldots, k+T_P$ is written as $k{:}k+T_P$.

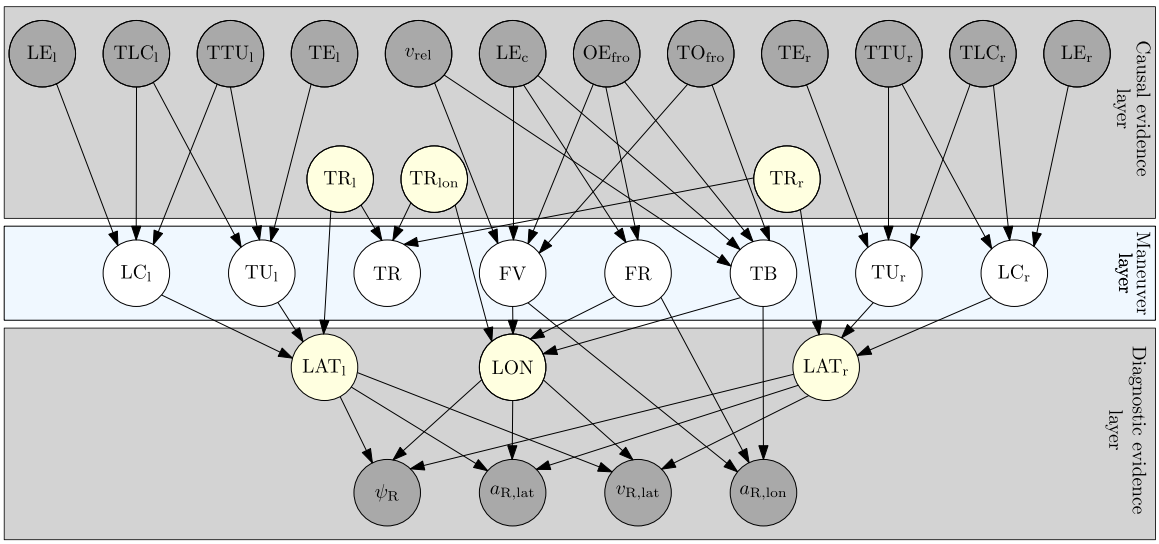

Fig. 3. Bayesian network for maneuver detection instantiated for each vehicle within the traffic scene at each time step k. Hidden maneuver nodes (blue) are inferred via Bayesian inference given causal and diagnostic evidence nodes (shaded). Helper nodes (yellow) are used to facilitate parameterization. Abbreviations are explained in Table I.

the detection and subsequent prediction of rare events. In contrast, we instantiate a separate network for every vehicle that primarily obtains evidences independent from other traffic participants. The last statement can be justified by thinking about, for example, adding the evidence that a neighboring vehicle occupies the ego vehicle's adjacent lane such as done in [14]. Then this evidence could only be reasonably included into the network in a way that it lowers the probability of an impending lane change for the ego vehicle due to the occupied adjacent lane. If weighted too strongly, this evidence would prevent the prediction of a collision if the ego vehicle indeed performed the unlikely lane change and is therefore intentionally not included in our network. As a result of these considerations, our network is designed under the implicit premise of drivers overlooking each other, at least, unless physical evidence contradicts this premise. An example for this is a vehicle already braking strongly in front of an obstacle. In this situation, the prediction of the timely stop prevents false warnings and is therefore incorporated.

The developed network is shown in Fig. 3. It consists of 8 binary (true and false) maneuver nodes within the maneuver layer (blue), 6 helper nodes (yellow), and 16 evidence nodes (shaded) summarized in Table I. All naturally continuous random variables, such as velocities, are discretized by dividing their values into several reasonable intervals. Thus, the complete network is discrete. We do not use either causal (predictive—from cause to effect as in [14]) or diagnostic (evidential—from effect to cause as in [12]) reasoning but both by embedding the hidden maneuver node layer in-between the observable causal and diagnostic evidence node layers, which additionally allows intercausal reasoning. The main consideration in the network design process is that the causal evidence layer models requirements for specific maneuvers to happen. The existence of a neighboring lane, for example, is a necessity for a lane change maneuver or the time until a turning is reached influences the probability of an upcoming turn maneuver. The diagnostic evidence layer, in contrast, models the maneuvers' consequences (symptoms) in form of measurable physical motion states. We use longitudinal and lateral vehicle acceleration $a_{R,\mathrm{lon/lat}}$, lateral velocity $v_{R,\mathrm{lat}}$, and yaw angle ψ_R within a road-fixed coordinate system [31] as diagnostic evidences, see Fig. 4. These are partly not directly connected with the maneuver layer but via helper nodes $\mathrm{LAT}_{l/r}$ and LON for lateral and longitudinal motion, respectively. This simplifies the parameterization of the corresponding conditional probability tables.

The combination of causal and diagnostic evidences allows explaining away. If, for example, the observed states of the diagnostic nodes are indistinguishable consequences of either a lane change or a turn maneuver, then the additional causal knowledge of a non-existing turning automatically raises the

TABLE I
RANDOM VARIABLES OF TYPE CAUSAL EVIDENCE (CE), DIAGNOSTIC EVIDENCE (DE), HELPER NODE (HN), AND MANEUVER NODE (MN)

Variable	Type	Explanation
LE$_{l/r/c}$	CE	Lane Existence left/right/current
TLC$_{l/r}$	CE	Time-To-Line crossing left/right
TTU$_{l/r}$	CE	Time-To-Turning left/right
TE$_{l/r}$	CE	Turning Existence left/right
v_{rel}	CE	Relative velocity to front object
OE$_{fro}$	CE	Front object existence
TO$_{fro}$	CE	Time-To-Front object
ψ_R	DE	Yaw angle to road tangent
$a_{R,lat}$	DE	Lateral acceleration perpendicular to road tangent
$v_{R,lat}$	DE	Lateral velocity perpendicular to road tangent
$a_{R,lon}$	DE	Longitudinal acceleration along road tangent
TR$_{l/lon/r}$	HN	Trash class helper left/longitudinal/right
LAT$_{l/r}$	HN	Lateral motion left/right
LON	HN	Longitudinal motion
LC$_{l/r}$	MN	Lane Change to the left/right
TU$_{l/r}$	MN	Turn to the left/right
TR	MN	Trash maneuver class (no maneuver)
FV	MN	Follow Vehicle
FR	MN	Follow Road
TB	MN	Target Brake

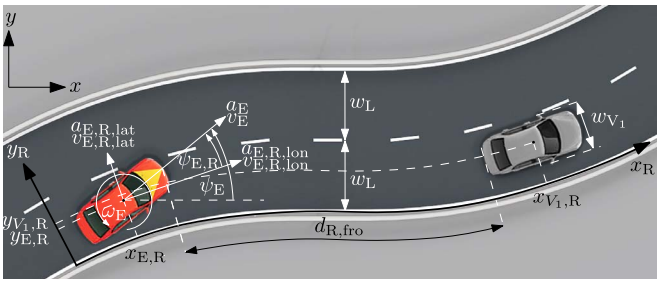

Fig. 4. Ego vehicle (red, index E) with vehicle in front (gray, index V_1) in road-fixed and global coordinate systems.

probability that the observed diagnostic evidence stems from a lane change. Moreover, the design approach allows to integrate a trash maneuver class TR for modeling all motions not belonging to a specific maneuver class, e.g. irrational movements of a drunken driver, by explaining away all contradictory evidence to the trash maneuver class via the helper nodes $\mathrm{TR}_{\mathrm{l/lon/r}}$. These are connected to TR in a noisy-or manner. The trash maneuver class also gets a high probability if all other maneuver requirements are missing, e.g. no lane or turning information is available such as in completely unstructured environments like parking zones or dirt tracks.

In every time step k, the network is updated with all available evidences. Uncertainties can be handled via soft evidences within this process [30]. Then, the individual maneuver nodes are normalized so that they form a single, valid, discrete maneuver random variable M with the 8 maneuver states and corresponding pmf $p(M)$.

B. Trajectory Prediction

For each maneuver, a prediction model is set up. Each model is adapted to the traffic scene by taking vehicle and environment evidences into account. They additionally contain random components to model different driving styles (prediction uncertainties) and are initialized with the current vehicle and environment state pdfs in each time step, which serve as a base for the prediction. These initial pdfs are supposed to be available from preceding algorithms, e.g. target trackers, in which measurement uncertainties are incorporated. Possible predicted trajectories of each maneuver class are qualitatively visualized in Fig. 5. Note that the presented models are not to be seen as the sole correct ones for the different predictions but rather as exemplary, working implementations, which can easily be replaced by arbitrary other stochastic processes due to the generality of the approach, e.g. by ones learned from human driving data [32].

1) Follow Road (FR): The model predicts the vehicle's longitudinal position along the road according to a (nearly) Constant Acceleration (CA) model, also called discrete Wiener process acceleration model [33], given by

$$\underbrace{\begin{pmatrix} x_{R,m+1} \\ v_{R,\mathrm{lon},m+1} \\ a_{R,\mathrm{lon},m+1} \end{pmatrix}}_{\boldsymbol{x}_{R,m+1}} = \underbrace{\begin{pmatrix} 1 & T & \frac{1}{2}T^2 \\ 0 & 1 & T \\ 0 & 0 & 1 \end{pmatrix}}_{\boldsymbol{A}_m} \underbrace{\begin{pmatrix} x_{R,m} \\ v_{R,\mathrm{lon},m} \\ a_{R,\mathrm{lon},m} \end{pmatrix}}_{\boldsymbol{x}_{R,m}} + \underbrace{\begin{pmatrix} \frac{1}{2}T^2 \\ T \\ 1 \end{pmatrix}}_{\boldsymbol{\gamma}_m} w_a \tag{1}$$

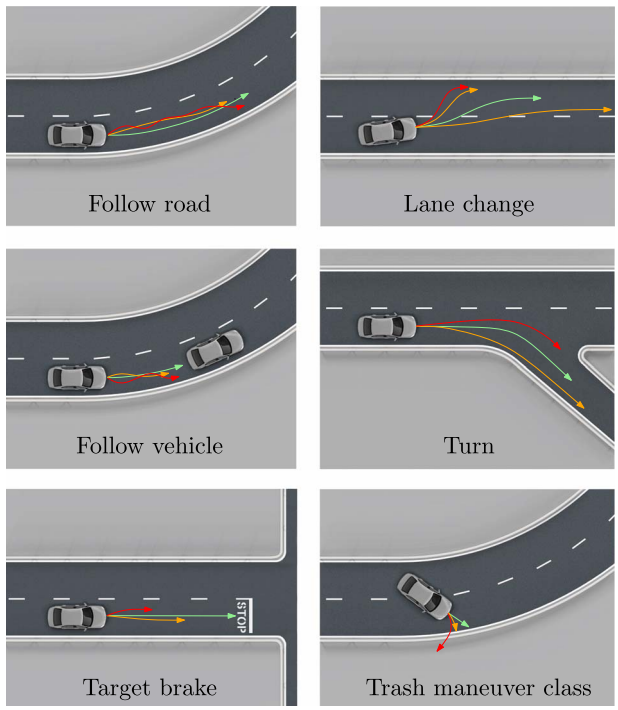

Fig. 5. Exemplary predicted trajectories of the maneuver-based prediction models. More probable predictions are shown in green, less probable ones in orange and red, respectively.

with state vector $\boldsymbol{x}_{R,m}$ including position $x_{R,m}$, longitudinal velocity $v_{R,\mathrm{lon},m}$, and acceleration $a_{R,\mathrm{lon},m}$ along the road, noise gain vector $\boldsymbol{\gamma}_m$, process noise scalar w_a, and prediction sampling time T within the prediction horizon $m \in \{k{:}k+T_P\}$. The noise corresponds to a zero-mean, white, Gaussian sequence representing acceleration increments, so that the covariance matrix of the process noise multiplied by the gain is given by

$$\boldsymbol{Q}_m = \boldsymbol{\gamma}_m \sigma^2_{\Delta a_{\mathrm{R,lon}}} \boldsymbol{\gamma}_m^T = \begin{pmatrix} \frac{1}{4}T^4 & \frac{1}{2}T^3 & \frac{1}{2}T^2 \\ \frac{1}{2}T^3 & T^2 & T \\ \frac{1}{2}T^2 & T & 1 \end{pmatrix} \sigma^2_{\Delta a_{\mathrm{R,lon}}}. \tag{2}$$

The predicted acceleration is therefore normally distributed around the current acceleration with linearly growing variance over the prediction horizon to model the rising uncertainty in the driver's acceleration profile the further we predict into the future. Negative velocities are suppressed as we do not want to predict that a decelerating vehicle moves backwards after braking to a standstill.

The vehicle's lateral position along the road $y_R(t)$ is modeled by an intuitively parameterizable, continuous-time Ornstein-Uhlenbeck process [33] described by the stochastic differential equation

$$\dot{y}_R(t) = -\alpha y_R(t) + \alpha u + w_c(t), \quad \alpha > 0 \tag{3}$$

with constant input scalar u for shifting the long-term mean and $w_c(t)$ being a zero-mean, white, Gaussian noise process with autocorrelation function $\mathbb{E}[w_c(t)w_c(t+\tau)] = Q_n\delta(\tau) = 2\alpha\sigma^2_{y_R}\delta(\tau)$ and constant noise intensity scalar Q_n.

The process has an exponentially decaying autocovariance function

$$\mathbb{E}\left[\left(y_R(t)-\bar{y}_R(t)\right)\left(y_R(t+\tau)-\bar{y}_R(t+\tau)\right)\right]=\sigma_{y_R}^2 e^{-\alpha|\tau|} \quad (4)$$

with $\bar{y}_R(\cdot)=\mathbb{E}[y_R(\cdot)]$ and time constant $T_c=1/\alpha$. The free parameters to be specified are u, T_c and σ_{y_R}. The long term mean is supposed to lie in the middle of the lane of width w_L, therefore $u=(1/2)w_L$. The time constant T_c affects the decay rate of the mean evolution and models how fast—on average—a vehicle currently not in the middle of the lane reaches the middle of the lane again. The parameter $\sigma_{y_R}^2$ equals the limiting value of the variance and is set in a way that a vehicle of width w_V driving in the middle of a lane of width w_L is completely inside the lane corresponds to the three sigma interval. The process (3) is discretized via zero-order hold, resulting in

$$y_{R,m+1}=e^{-\alpha T}y_{R,m}+(1-e^{-\alpha T})u+w_{y_R}, \forall\, m\in\{k{:}k+T_P\} \quad (5)$$

with process noise scalar w_{y_R} with variance $Q_m=\sigma_{y_R}^2(1-e^{-2\alpha T})$. The advantageous properties for suggesting the Ornstein-Uhlenbeck process for lateral vehicle position prediction are i) the growing variance to model the rising uncertainty of the future lateral vehicle position, ii) the boundedness of the variance with respect to the lane width, which prevents false warnings, e.g. in the case of an oncoming vehicle on an adjacent lane, and iii) the stochastic dependence between future time steps that prevents unrealistic sudden jumps in lateral position.

The yaw angle along the road is modeled as normally distributed around zero with small allowed deviations as the vehicle's orientation is supposed to nearly correspond to the road orientation in a FR maneuver. Thus, it reads

$$p(\psi_{R,m}|M=\text{FR})=\mathcal{N}\left(0,\sigma_{\psi_R}^2\right), \forall\, m\in\{k:k+T_P\}. \quad (6)$$

The corresponding joint distributions over the prediction horizon can now be derived straightforwardly. The longitudinal joint distribution $p(\boldsymbol{x}_{R,k:k+T_\text{p}}|M=\text{FR})$ is given by

$$p(\boldsymbol{x}_{R,k:k+T_\text{p}}|M=\text{FR})=p(\boldsymbol{x}_{R,k})\prod_{m=k}^{k+T_\text{p}-1}p(\boldsymbol{x}_{R,m+1}|\boldsymbol{x}_{R,m}) \quad (7)$$

with $p(\boldsymbol{x}_{R,m+1}|\boldsymbol{x}_{R,m})=\mathcal{N}(\boldsymbol{A}_m\boldsymbol{x}_{R,m},\boldsymbol{Q}_m)$ because of the first-order Markov property of the linear CA model.[2] The lateral position joint distribution is analogously given by

$$p(y_{R,k:k+T_\text{p}}|M=\text{FR})=p(y_{R,k})\prod_{m=k}^{k+T_\text{p}-1}p(y_{R,m+1}|y_{R,m}) \quad (8)$$

with $p(y_{R,m+1}|y_{R,m})=\mathcal{N}(e^{-\alpha T}y_{R,m}+(1-e^{-\alpha T})u, Q_m)$, whereas the yaw angle joint distribution follows

$$p(\psi_{R,k:k+T_\text{p}}|M=\text{FR})=\prod_{m=k}^{k+T_\text{p}}p(\psi_{R,m}|M=\text{FR}) \quad (9)$$

due to a simplistic stochastic independence assumption.

[2]The notation $p(\boldsymbol{x})=\mathcal{N}(\boldsymbol{\mu},\boldsymbol{P})$ is used for a multivariate Gaussian pdf of a random vector $\boldsymbol{x}$ with mean $\boldsymbol{\mu}$ and covariance $\boldsymbol{P}$.

2) Follow Vehicle (FV): The model is based on the assumption that the driver reacts to another vehicle in front and accelerates comfortably in a way that an adequate mean reference time gap τ_r occurs in the near future. It assumes moderate reaction of the driver similar to adaptive cruise control systems [34] and does therefore not predict abrupt braking or acceleration maneuvers. The model can predict collisions if the driver reacts to a vehicle in front too slightly. It can also suppress false warnings in situations in which a FR maneuver might already falsely predict a collision, e.g. if a driver reacts moderately to vehicles further away. The acceleration distribution along the road is modeled as normally distributed around an assumed mean reference acceleration

$$a_{R,\text{lon,r},m}=\begin{cases}c_\text{FV}(\Delta\tau_m)a_{f,\min}, & \Delta\tau_m<0\\ c_\text{FV}(\Delta\tau_m)a_{f,\max}, & \Delta\tau_m\geq 0\end{cases} \quad (10)$$

which depends on the difference between predicted time gap τ_m and the assumed mean reference time gap τ_r, $\Delta\tau_m=\tau_m-\tau_r$, with τ_m given by[3] $\tau_m=d_{R,\text{fro},m}/v_{R,\text{lon},m}$, with distance to the front vehicle $d_{R,\text{fro},m}$ and scaling function

$$c_\text{FV}(\Delta\tau_m)=\min\left(1;\frac{\Delta\tau_m^2}{2\tau_{m\text{S}}}\right), \forall\, m\in\{k:k+T_P\}. \quad (11)$$

This scaling function models how much the driver exploits the assumed minimum and maximum comfort acceleration, $a_{f,\min}$ and $a_{f,\max}$, in dependence on the predicted time gap and its deviation from the reference time gap. It is based on the assumption that a driver will accelerate smoothly in the case of positive time gap differences but decelerate more strongly in the case of negative $\Delta\tau$. The rising uncertainties in the so-calculated mean reference accelerations are again modeled by a linearly growing acceleration variance over the prediction horizon via $a_{R,\text{lon},m}=a_{R,\text{lon,r},m}+\tilde{a}_{R,\text{lon},m}, \forall\, m\in\{k:k+T_P\}$, in which $\tilde{a}_{R,\text{lon},m}$ follows the discrete Wiener process $\tilde{a}_{R,\text{lon},m+1}=\tilde{a}_{R,\text{lon},m}+w_a$ with white, Gaussian noise scalar w_a with variance $\sigma_{\Delta a_{R,\text{lon}}}^2$ and $\tilde{a}_{R,\text{lon},k}=0$. Velocities and positions along the road are given by integration, lateral position and yaw angle distributions are modeled analogous to the FR maneuver, negative velocities are suppressed.

3) Target Brake (TB): The model predicts under the assumption that the vehicle stops in front of a braking target, such as an obstacle, another vehicle, a stop line, or a red traffic light. The predicted acceleration equals the necessary constant acceleration for the vehicle with current velocity $v_{R,\text{lon},k}$ to stop in a specific safety distance Δd to the braking target under consideration of an achievable minimum acceleration a_min, therefore

$$a_{R,\text{lon},m}=\max\left(\frac{-v_{R,\text{lon},k}^2}{2(d_{R,\text{fro},k}-\Delta d)};a_\text{min}\right), \forall\, m\in\{k:k+T_P\} \quad (12)$$

in which the current distance to the target is given by $d_{R,\text{fro},k}$. The safety distance is treated as normally distributed around

[3]For the prediction of the time gap evolution, the preceding vehicle's position is calculated under a constant velocity assumption.

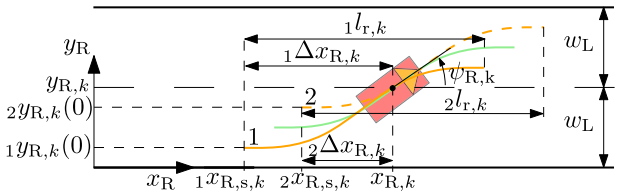

Fig. 6. Lane change maneuver model for a given vehicle configuration at time step k with relevant quantities shown on two predicted trajectory samples.

a mean reference safety distance d_r with a standard deviation designed in a way that a vehicle stopping directly in front of the braking target with no safety margin corresponds to the three sigma interval, therefore $p(\Delta d|M=\text{TB}) = \mathcal{N}(d_r, (d_r/3)^2)$. Lateral position and yaw angle distributions are modeled analogous to the FR maneuver, negative velocities are again suppressed.

4) Lane Change (LC): The model predicts lane changes according to a prototype model that is represented by a sine half-cycle in road coordinates,

$$y_R(\Delta x_R) = \frac{w_L}{2}\sin\left(\frac{\pi}{l_r}\Delta x_R - \frac{\pi}{2}\right) + w_L, \forall\, \Delta x_R \in [0, l_r] \tag{13}$$

with $\Delta x_R = x_R - x_{R,\text{s}}$, maneuver start coordinate $x_{R,\text{s}}$, width of each lane w_L, reference maneuver length l_r, and derivative

$$\begin{aligned}\psi_R &= \arctan\left(\frac{dy_R(\Delta x_R)}{d(\Delta x_R)}\right)\\ &= \arctan\left(\frac{w_L\pi}{2l_r}\cos\left(\frac{\pi}{l_r}\Delta x_R - \frac{\pi}{2}\right)\right), \forall\, \Delta x_R \in [0, l_r].\end{aligned} \tag{14}$$

This model is adapted to the current lateral vehicle position and yaw angle state at each time step k by setting $y_R{=}y_{R,k}$ and $\psi_R{=}\psi_{R,k}$ in (13) and (14) and solving for $l_{r,k}$ and $\Delta x_{R,k}$, which results in

$$\begin{aligned} l_{r,k} &= \frac{w_L\pi}{2\tan\psi_{R,k}}\cos\left(\arcsin\left(\frac{2y_{R,k}}{w_L} - 2\right)\right)\\ \Delta x_{R,k} &= \left(\frac{1}{2} + \frac{1}{\pi}\arcsin\left(\frac{2y_{R,k}}{w_L} - 2\right)\right) l_{r,k}\end{aligned} \tag{15}$$

to get the remaining maneuver length $l_{r,k} - \Delta x_{R,k}$ for the prediction. Uncertainties are introduced by modeling the lateral maneuver origin for these calculations as normally distributed around the middle of the lane with $p(y_{R,k}(\Delta x_{R,k}=0)) = \mathcal{N}((w_L/2), \sigma^2_{y_{R,s}})$. Consequently, the quantities $l_{r,k}$, $\Delta x_{R,k}$, and $x_{\text{R,s,k}}$ also become random variables.[4] Fig. 6 visualizes the mentioned quantities on two exemplary trajectory samples. The prediction itself is carried out with the so-adapted prototype model. The uncertain acceleration along the curve is modeled as a discrete Wiener process analogous to the FR model. After double integration and transformation to the road coordinate system, this gives the function arguments of (13) and (14) for the uncertain prediction of y_R and ψ_R. As soon as the end of the sine half-cycle is reached, the prediction is carried out with the FR model for the remaining prediction horizon.

[4]Note that this is just a method to obtain uncertain predictions consistent with the current vehicle configuration and does not imply that the vehicle has truly been on one of the resulting trajectories in the past.

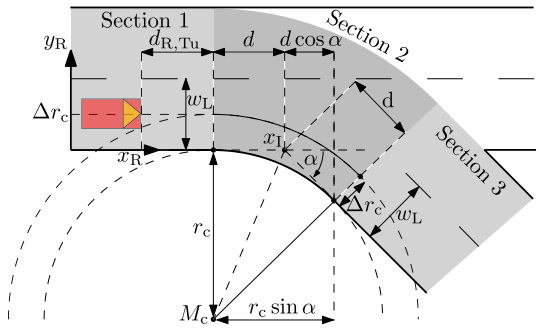

Fig. 7. Turn maneuver sections.

5) Turn (TU): The model predicts turns by partitioning the maneuver into three sections: i) before the turn on the initial road, ii) the turn itself, and iii) the remaining prediction on the destination road after the turn is complete. The initial and the destination road are considered straight in the vicinity of the turn, the destination road is rotated versus the initial road by the angle $\alpha \in]0, \pi[$. The right road border[5] is supposed to follow a circular arc $(x_R - x_c)^2 + (y_R - y_c)^2 = r_c^2$ during the road transition with radius r_c and center $M_c = (x_c, y_c)$, sketched in Fig. 7.

In the first section, lateral and longitudinal predictions are performed analogous to the FR model with the difference that the predicted longitudinal acceleration is considered normally distributed around a constant reference acceleration $a_{R,\text{lon,r},m}$ over the prediction horizon. This reference acceleration is calculated as the necessary constant acceleration that ensures that a maximum velocity $v_{R,\text{lon,max}}$ is not exceeded at the start of the turn according to

$$a_{R,\text{lon,r},m} = \begin{cases} \tilde{a} = \max\left(\frac{v_{\text{lon},k}\Delta v_k + \frac{1}{2}\Delta v_k^2}{d_{R,\text{Tu},k}}; a_{\min}\right), & \tilde{a} < a_{R,\text{lon},k} \\ a_{R,\text{lon},k}, & \text{else} \end{cases} \tag{16}$$

with $\Delta v_k = v_{R,\text{lon,max}} - v_{\text{lon},k}$, remaining distance to the turn $d_{R,\text{Tu},k}$, and minimum acceleration $a_{\min}$. If the current acceleration does not result in an exceeding of $v_{R,\text{lon,max}}$, the current acceleration value is used for prediction instead. The maximum velocity itself is determined under the assumption that a driver only exposes himself to a maximum centripetal acceleration $a_{c,\max}$ during the turn phase, so that $v_{R,\text{lon,max}} = \sqrt{a_{\text{c,max}}(r_c + \Delta r_c)}$ holds, under consideration of a constant velocity model in this second section. Here, the circular arc's center lies on the angle bisector between the two road tangents. The radius is adapted to the road geometry so that initial and destination roads' right borders are also tangents of the circle. For the calculation of M_c and r_c, we consider the distance d between the start/end of the rounded road transition and the intersection point's longitudinal road coordinate x_I of the two road tangents as known and consequently reach

[5]We limit the explanations to the turn right maneuver.

$r_c = d(1+\cos\alpha)/(\sin\alpha)$ and $y_c = -r_c$. The prediction itself is performed by considering the lateral positions on the initial and destination road as random variables following a normal distribution around the middle of the road to model different turn executions as every driver cuts the corner differently. The predicted circular paths are therefore given by $(x_R - x_c)^2 + (y_R - y_c)^2 = (r_c + \Delta r_c)^2$, with $p(\Delta r_c) = \mathcal{N}((w_L/2), \sigma_{y_R}^2)$. The third section is again predicted with the FR maneuver model, which is initialized with the final values of the second section.

6) Trash Maneuver Class (TR): The model predicts the motion according to a (nearly) Constant Turn Rate and Acceleration model [13] (CTRA) with

$$\begin{pmatrix} x_{m+1} \\ y_{m+1} \\ \psi_{m+1} \\ v_{m+1} \\ a_{m+1} \\ \omega_{m+1} \end{pmatrix} = \begin{pmatrix} x_m + \tilde{x}_m \\ y_m + \tilde{y}_m \\ \psi_m + \omega_m T \\ v_m + a_m T \\ a_m \\ \omega_m \end{pmatrix} + \boldsymbol{w}_m, \forall\, m \in \{k{:}k{+}T_P\} \tag{17}$$

$$\begin{aligned} \tilde{x}_m =& \frac{1}{\omega_m^2}\left[(v_m\omega_m + a_m\omega_m T)\sin(\psi_m + \omega_m T)\right. \\ &\left. + a_m\cos(\psi_m + \omega_m T) - v_m\omega_m\sin\psi_m - a_m\cos\psi_m\right] \\ \tilde{y}_m =& \frac{1}{\omega_m^2}\left[(-v_m\omega_m - a_m\omega_m T)\cos(\psi_m + \omega_m T)\right. \\ &\left. + a_m\sin(\psi_m + \omega_m T) + v_m\omega_m\cos\psi_m - a_m\sin\psi_m\right] \end{aligned} \tag{18}$$

with global position x_m, y_m, yaw angle ψ_m, yaw rate ω_m, and velocity and acceleration magnitude in driving direction v_m and a_m, respectively. The noise with process noise vector $\boldsymbol{w}_m$ corresponds to a zero-mean, white, Gaussian sequence representing acceleration and yaw rate increments with covariance matrix $\boldsymbol{Q}_m = \mathrm{diag}(0;0;0;0;\sigma_{\Delta a}^2;\sigma_{\Delta\omega}^2)$. The model is purely based on physical vehicle states. It can thus also be employed if no environment knowledge is available and is used if the vehicle motion does not correspond to any other driving maneuver.

7) Maneuver Model Combination: Every maneuver prediction model therefore generates, after transformation to a common, global reference frame, a joint pdf $p(\boldsymbol{x}_{k:k+T_P}|M_{j,k})$ over the prediction horizon with configuration $\boldsymbol{x} = (x, y, \psi)^T$ for all $j \in \{1, \ldots, r\}$ maneuvers for each vehicle. By marginalizing out the maneuver states from the combined pdf $p(\boldsymbol{x}_{E,k:k+T_P}, M_k)$ with the help of $p(M_{E,k})$ and $p(M_{V_i,k})$ from the Bayesian network inference result of Section III-A, we reach

$$\begin{aligned} p(\boldsymbol{x}_{E,k:k+T_P}) &= \sum_{j=1}^{r} p(\boldsymbol{x}_{E,k:k+T_P}|M_{E,k}=j)p(M_{E,k}=j) \\ p(\boldsymbol{x}_{V_i,k:k+T_P}) &= \sum_{j=1}^{r} p(\boldsymbol{x}_{V_i,k:k+T_P}|M_{V_i,k}=j)p(M_{V_i,k}=j) \end{aligned} \tag{19}$$

for the ego vehicle and the other $i \in \{1, \ldots, f\}$ vehicles, respectively. The emerging densities are thus a combination of all prediction models that are weighted with their current maneuver probabilities. These densities are used for criticality assessment in the following.

C. Criticality Assessment

1) Dynamic Environment: In [35], a general formula for probabilistic collision checking is presented which, however, only holds for calculating the collision probability of two uncertain, extended objects at a specific point in time. Adapted to our case, the probability of the event C_I: *The ego vehicle collides exactly with vehicle V_i at a specific, common instant of time*, is given by[6] [35]

$$p(C_I) = \int_{\boldsymbol{x}_{V_i}} \int_{\boldsymbol{x}_E} I_{C_I}(\boldsymbol{x}_E, \boldsymbol{x}_{V_i}) p(\boldsymbol{x}_E, \boldsymbol{x}_{V_i}) d\boldsymbol{x}_E d\boldsymbol{x}_{V_i} \tag{20}$$

with joint density over the uncertain configurations of both vehicles $p(\boldsymbol{x}_E, \boldsymbol{x}_{V_i})$ and collision indicator function

$$I_{C_I}(\boldsymbol{x}_E, \boldsymbol{x}_{V_i}) = \begin{cases} 1, & \mathcal{S}(\boldsymbol{x}_E) \bigcap \mathcal{S}(\boldsymbol{x}_{V_i}) \neq \emptyset \\ 0, & \text{else.} \end{cases} \tag{21}$$

Here, $\mathcal{S}(\boldsymbol{x}_E)$ and $\mathcal{S}(\boldsymbol{x}_{V_i})$ refer to the set of points in space that are occupied by the ego and obstacle vehicle when their configurations are given by $\boldsymbol{x}_E$ and $\boldsymbol{x}_{V_i}$, respectively. For criticality assessment over a future time span, i.e. the calculation of the probability of the event $C_{V_i,k}(T_P)$: *The ego vehicle collides with vehicle V_i at least once within the prediction horizon* $m \in \{k : k + T_P\}$, evaluated at time step k, the formula has to be generalized as follows:

$$\begin{aligned} p(C_{V_i,k}(T_P)) = & \int_{\boldsymbol{x}_{V_i,k+T_P}} \int_{\boldsymbol{x}_{E,k+T_P}} \cdots \int_{\boldsymbol{x}_{V_i,k}} \int_{\boldsymbol{x}_{E,k}} \\ & I_C(\boldsymbol{x}_{E,k:k+T_P}, \boldsymbol{x}_{V_i,k:k+T_P}) p(\boldsymbol{x}_{E,k:k+T_P}, \boldsymbol{x}_{V_i,k:k+T_P}) \\ & d\boldsymbol{x}_{E,k} d\boldsymbol{x}_{V_i,k}, \ldots, d\boldsymbol{x}_{E,k+T_P} d\boldsymbol{x}_{V_i,k+T_P} \end{aligned} \tag{22}$$

with new, modified collision indicator function

$$I_C(\boldsymbol{x}_{E,k:k+T_P}, \boldsymbol{x}_{V_i,k:k+T_P}) = \begin{cases} 1, & \exists m \in \{k{:}k{+}T_P\} : \\ & \mathcal{S}(\boldsymbol{x}_{E,m}) \bigcap \mathcal{S}(\boldsymbol{x}_{V_i,m}) \neq \emptyset \\ 0, & \text{else.} \end{cases} \tag{23}$$

Therefore, an integration of the joint density of both vehicles' configurations of all future time steps, $p(\boldsymbol{x}_{E,k:k+T_P}, \boldsymbol{x}_{V_i,k:k+T_P})$, is necessary. This integration needs to be performed over a volume that is defined by the modified collision indicator function, which in turn is equal to one if there exists at least one time step in the prediction horizon in which the occupancy sets of the specific vehicle configurations overlap, i.e. a predicted collision occurs. Note that just considering the marginal densities $p(\boldsymbol{x}_{E,k}, \boldsymbol{x}_{V_i,k}), p(\boldsymbol{x}_{E,k+1}, \boldsymbol{x}_{V_i,k+1}), \ldots, p(\boldsymbol{x}_{E,k+T_P}, \boldsymbol{x}_{V_i,k+T_P})$ is insufficient for the calculation of the event probability as the same marginal prediction densities can lead to different $p(C_{V_i,k}(T_P))$, see the example in Fig. 8.

[6]The short notation $\int_{\boldsymbol{x}}(.)d\boldsymbol{x}$ means integration over the whole range of $\boldsymbol{x}$. For example, if $\boldsymbol{x} = (x_1, \ldots, x_n)^T \in \mathbb{R}^n$, then $\int_{\boldsymbol{x}}(.)d\boldsymbol{x} = \int_{\mathbb{R}^n}(.)d\boldsymbol{x}$.

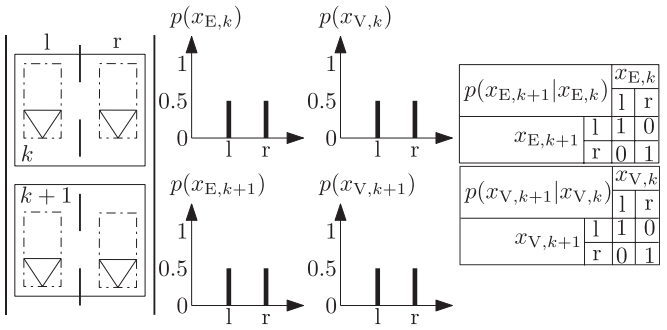

Fig. 8. Example showing that identical marginal prediction densities can lead to different collision event probabilities. We suppose that two vehicles, E and V, have independent trajectories and are either on the left (state l) or on the right (state r) lane at each of the two considered time steps k and $k+1$. The vehicles collide if they are on the same lane at the same time. The fictive marginal pmfs of both time steps and vehicles are given in the middle. Each vehicle is thus on the left or right lane with equal probability of 0.5 at both time steps. First, we consider each vehicle's positions over time as independent, therefore uncorrelated, random variables. In this case, the probability of at least one collision within the time interval $\{k{:}k+T_P\} = \{k, k+1\}$ is straightforwardly given by $p(C_{V,k}(T_P)) = 1-(0.5^2+0.5^2)^2 = 0.75$, i.e. as one minus the product of no collision in both steps. In contrast, we now consider the lane positions of each vehicle over time to be dependent, perfectly correlated random variables with transition probabilities given on the right. Each vehicle is thus modeled as staying on the same lane for both time steps. The marginal pmfs remain the same, whereas the event probability now changes to $p(C_{V,k}(T_P)) = 0.5^2+0.5^2 = 0.5$ as a collision in one time step now automatically results in a collision in the next.

We further consider the trajectories of all vehicles as independent.[7] Therefore the joint density in (22) reduces to

$$p(\boldsymbol{x}_{E,k:k+T_P}, \boldsymbol{x}_{V_i,k:k+T_P}) = p(\boldsymbol{x}_{E,k:k+T_P}) p(\boldsymbol{x}_{V_i,k:k+T_P}) \tag{24}$$

with the pdfs on the right hand side given by (19). For the evaluation of the indicator function I_C, the vehicles' oriented bounding rectangles are analytically checked for overlap with the help of the separating axes theorem. For performance reasons, this is accompanied by a fast preliminary collision check between the corresponding bounding circles.

2) Static Environment: So far, only other dynamic vehicles have been considered for criticality assessment. For a comprehensive system, however, also static obstacles need to be taken into account. In the following, it is shown how a compact Parametric Free Space (PFS) map representation [36]–[38] for the static driving environment can be advantageously embedded into the concept. For better understanding, the main properties of PFS maps are shortly outlined. PFS maps can be extracted from the well-known occupancy grid maps after elimination of dynamic object corruptions [38]–[40]. They provide a compact representation of the reachable, drivable free space and consist of a parametric, closed B-spline curve $\boldsymbol{r}(s) \in \mathbb{R}^2$ given by

$$\boldsymbol{r}(s) = \begin{pmatrix} x(s) \\ y(s) \end{pmatrix} = \begin{pmatrix} \boldsymbol{b}(s)^T & \boldsymbol{0} \\ \boldsymbol{0} & \boldsymbol{b}(s)^T \end{pmatrix} \boldsymbol{x}_P, \forall\, s \in [0, L] \tag{25}$$

[7]As mentioned already, otherwise, a collision prediction is hardly possible as the necessary modeling of the combined traffic scene pdf would require the postulation of sensible individual drivers that try not to collide.

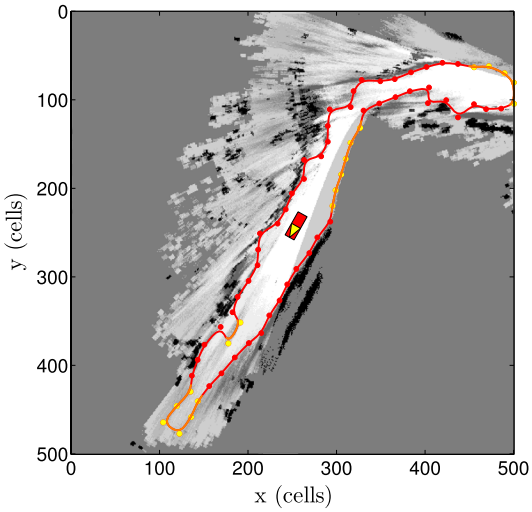

Fig. 9. Exemplary PFS map (colored) overlaid corresponding occupancy grid map (gray).

with B-spline coordinate functions $x(s)$ and $y(s)$, the vector of N_B B-spline basis functions

$$\boldsymbol{b}(s) = (B_0(s) B_1(s), \ldots, B_{N_\mathrm{B}-1}(s))^T \in \mathbb{R}^{N_\mathrm{B}} \tag{26}$$

and the B-spline control vector

$$\boldsymbol{x}_P = (q_{x,0}, \ldots, q_{x,N_\mathrm{B}-1} q_{y,0}, \ldots, q_{y,N_\mathrm{B}-1})^T \in \mathbb{R}^{2N_\mathrm{B}} \tag{27}$$

made up from control points or de Boor points $(q_{x,i}, q_{y,i})$ [41]. Each B-spline coordinate function is a piecewise polynomial function that consists of $L \in \mathbb{N}$ concatenated polynomial segments, the so-called spans S_m with $m \in \{0, \ldots, L-1\}$ of order $d \in \mathbb{N}$, joined together at breakpoints. Basis functions for a B-spline function with N_k knots at $k_0 \le k_1 \le \cdots \le k_{N_k-1}$ can be constructed by a recursion formula with the ground instance

$$B_{n,1}(s) = \begin{cases} 1, & \text{if } k_n \le s < k_n + 1 \\ 0, & \text{otherwise} \end{cases} \tag{28}$$

and the inductive step

$$B_{n,d}(s) = \frac{(s-k_n) B_{n,d-1}(s)}{k_{n+d-1} - k_n} + \frac{(k_{n+d} - s) B_{n+1,d-1}(s)}{k_{n+d} - k_{n+1}} \tag{29}$$

with summands being zero if the denominator vanishes [41]. If the knot spacing is uniform, the B-spline is called uniform as well, otherwise non-uniform. To get closed curves within the PFS map, the basis functions have to be taken periodic over the interval $[0, L]$. This curve represents the—for the ego vehicle—reachable outer free space boundary, which can either be a delimiter to real obstacles or to unknown, not yet observed, environment areas. An example is shown in the motivating Fig. 1 as well as in Fig. 9 with obstacle boundaries visualized in red and unknown environment boundaries in orange. Inner free space boundaries in the PFS map are, in contrast, described by geometric primitives in form of N_c circles with state $\boldsymbol{x}_c \in \mathbb{R}^3$

and N_r oriented rectangles with state $\boldsymbol{x}_r \in \mathbb{R}^5$. The PFS map's state

$$\boldsymbol{x}_{\mathrm{PFS},k} = \left(\boldsymbol{x}_P^T \boldsymbol{x}_{c,1}^T, \ldots, \boldsymbol{x}_{c,N_c}^T \boldsymbol{x}_{r,1}^T, \ldots, \boldsymbol{x}_{r,N_r}^T\right)^T \in \mathbb{R}^{2N_b+3N_c+5N_r} \tag{30}$$

at time step k is a combination of the states of the outer and inner boundaries. Note that the PFS map is constant over the prediction horizon as the static environment does not change. We additionally consider the PFS map as deterministic because uncertainties of the static environment are much smaller than the rising uncertainties involved in the future motion of other dynamic vehicles. Therefore, the collision probability of the event $C_{\mathrm{PFS},k}(T_P)$: *The ego vehicle collides with the static driving environment at least once within the prediction horizon* $\{k{:}k+T_P\}$, evaluated at time step k, is given by

$$p(C_{\mathrm{PFS},k}(T_P)) = \int_{\boldsymbol{x}_{E,k+T_P}} \cdots \int_{\boldsymbol{x}_{E,k}} I_{C_{\mathrm{PFS}}}(\boldsymbol{x}_{E,k:k+T_P}) \, p(\boldsymbol{x}_{E,k:k+T_P}) d\boldsymbol{x}_{E,k}, \ldots, d\boldsymbol{x}_{E,k+T_P} \tag{31}$$

with collision indicator function

$$I_{C_{\mathrm{PFS}}}(\boldsymbol{x}_{E,k:k+T_P}) = \begin{cases} 1, & \exists m \in \{k{:}k+T_P\} : \\ & \mathcal{S}(\boldsymbol{x}_{E,m}) \bigcap \mathcal{S}(\boldsymbol{x}_{\mathrm{PFS},k}) \neq \emptyset \\ 0, & \text{else} \end{cases} \tag{32}$$

in which $\mathcal{S}(\boldsymbol{x}_{\mathrm{PFS},k})$ describes the set of points within the PFS map that are obstacle boundary delimiters. We only need to integrate the ego vehicle's joint pdf over the specified volume in this case. If the uncertainties in PFS maps with pdf $p(\boldsymbol{x}_{\mathrm{PFS},k})$ should be considered, then (31) generalizes to

$$p\left(C_{\mathrm{PFS},k}(T_P)\right) = \int_{\boldsymbol{x}_{\mathrm{PFS},k}} \int_{\boldsymbol{x}_{E,k+T_P}} \cdots \int_{\boldsymbol{x}_{E,k}} I_{C_{\mathrm{PFS}}}(\boldsymbol{x}_{E,k:k+T_P}, \boldsymbol{x}_{\mathrm{PFS},k}) \, p(\boldsymbol{x}_{E,k:k+T_P}, \boldsymbol{x}_{\mathrm{PFS}_k}) d\boldsymbol{x}_{E,k}, \ldots, d\boldsymbol{x}_{E,k+T_P} d\boldsymbol{x}_{\mathrm{PFS},k} \tag{33}$$

with identical indicator function. This indicator function is evaluated by analytically checking whether the predicted ego vehicle's bounding rectangle overlaps with $\mathcal{S}(\boldsymbol{x}_{\mathrm{PFS},k})$. For the collision detection with the outer free space boundary described by the B-Spline curve, this evaluation can be done by checking whether at least one of the line segments

$$\boldsymbol{l}_i(s_l) = \begin{pmatrix} x_l(s_l) \\ y_l(s_l) \end{pmatrix} = \begin{pmatrix} C_{x,i} \\ C_{y,i} \end{pmatrix} + s_l \begin{pmatrix} C_{x,i+1} - C_{x,i} \\ C_{y,i+1} - C_{y,i} \end{pmatrix} \forall\, s_l \in [0,1] \tag{34}$$

between the ego vehicle's $i \in \{1, \ldots, 4\}$ corners points $C_i = (C_{x,i}, C_{y,i})$ with $C_1 = C_5$ and the B-spline curve $\boldsymbol{r}(s)$ intersect. Considering uniform, quadratic $(d = 3)$, periodic B-spline basis functions, therefore $L = N_b = N_k - 1$ and $\{k_0, \ldots, k_{N_k-1}\} = \{0, \ldots, L\}$, then the B-spline curve within span S_m is given by

$$\boldsymbol{r}_m(\Delta s) = \begin{pmatrix} x_m(\Delta s) \\ y_m(\Delta s) \end{pmatrix} = \begin{pmatrix} \boldsymbol{b}_m(\Delta s)^T & \boldsymbol{0} \\ \boldsymbol{0} & \boldsymbol{b}_m(\Delta s)^T \end{pmatrix} \boldsymbol{x}_{P,m} \tag{35}$$

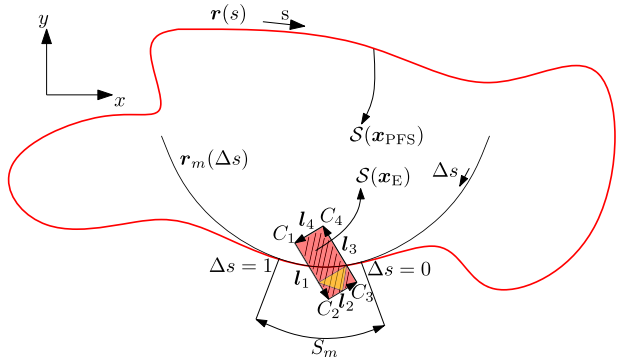

Fig. 10. Collision check between the B-spline curve and the ego vehicle bounding rectangle.

with

$$\boldsymbol{b}_m(\Delta s) = \begin{pmatrix} \frac{1}{2}\Delta s^2 - \Delta s + \frac{1}{2} \\ -\Delta s^2 + \Delta s + \frac{1}{2} \\ \frac{1}{2}\Delta s^2 \end{pmatrix} \in \mathbb{R}^3, \forall\, \Delta s \in [0,1] \tag{36}$$

and $\boldsymbol{x}_{P,m} = (q_{x,m-2}\ q_{x,m-1}\ q_{x,m} q_{y,m-2}\ q_{y,m-1}\ q_{y,m}{}^T) \in \mathbb{R}^6$ with $m \in \{0, \ldots, L-1\}$, $q_{x,-2} = q_{x,L-2}, q_{y,-2} = q_{y,L-2}$, $q_{x,-1} = q_{x,L-1}, q_{y,-1} = q_{y,L-1}$ due to the periodicity, and $\Delta s = s - k_m$. For collision checking, we solve the system of quadratic equations

$$\boldsymbol{l}_i(s_l) = \boldsymbol{r}_m(\Delta s), \forall\, i \in \{1, \ldots, 4\} \text{ and } m \in \{0, \ldots, L-1\} \tag{37}$$

for real solutions of Δs and s_l, which both have to be inside the interval [0,1] for an occurring collision. Fig. 10 visualizes the relations.

The collision detection with the rectangular and circular inner free space boundaries is realized analogously to the collision detection with other predicted vehicles. The advantage of using these PFS maps for criticality assessment is that arbitrary static environment structures can be embedded in the criticality assessment part analytically, and the complete static environment can be checked for collisions with the future ego vehicle configurations in the same way.

3) Combination: Considering all f predicted vehicles and the static environment, the probability of the combined event $C_k(T_P)$: *The ego vehicle collides with at least one vehicle or the static driving environment at least once within the prediction horizon* $\{k{:}k+T_P\}$, evaluated at time step k, can now be calculated as

$$\begin{aligned} p(C_k(T_P)) &= p\left(\bigcup_{i=1}^{f} C_{V_i,k}(T_P) \cup C_{\mathrm{PFS},k}(T_P)\right) \\ &= p\left(\neg\left(\bigcap_{i=1}^{f} \neg C_{V_i,k}(T_P) \cap \neg C_{\mathrm{PFS},k}(T_P)\right)\right) \\ &= 1 - \prod_{i=1}^{f} \left(1 - p\left(C_{V_i,k}(T_P)\right)\right)\left(1 - p(C_{\mathrm{PFS},k}(T_P))\right) \end{aligned} \tag{38}$$

in which the last step follows from the stochastic independence of the individual collision events. This independence is a consequence of the independence assumption of all vehicle

trajectories, so that the probability of the ego vehicle colliding with one object is not influenced by the probability of colliding with another. If this assumption is omitted, then $p(C_k(T_P))$ must be calculated according to (39), shown at the bottom of the page. Note that the last factor in (38) already refers to the complete static driving environment independent of the number of static obstacles due to the PFS map.

4) TTCCP: We now consider (38) as a function of T_P, i.e. the length of the prediction horizon (number of prediction time steps), and define the criticality metric TTCCP as the time until the combined collision probability $p(C_k(T_P))$ exceeds a Critical Collision Probability (CCP), therefore

$$\text{TTCCP} = \min\left(T_P | p\left(C_k(T_P)\right) > \text{CCP}\right) \cdot T \tag{40}$$

with prediction sampling time T. This can be seen as a generalization of the TTC in arbitrary, uncertain, multi-object driving environments. Note that the TTCCP is based on the collision probability over a future time span and not on the collision probability of future time instants. The former is always a monotonically increasing function over the prediction time, which does not hold for the latter. This is also the reason why a CCP threshold on the collision probability of future time instants is a suboptimal approach to calculate the TTCCP. This probability can be low in every prediction time step and thus falsely indicate a safe situation, whereas the collision probability over a time span can reveal an imminent danger by combining the individual criticalities over time, which is further illustrated in Fig. 11.

5) Monte Carlo Simulation: In a practical implementation, (22) and (31) are solved via Monte Carlo simulation. Therefore, the expectation of the indicator function in (22), i.e. the collision probability, can be estimated by

$$p\left(C_{V_i,k}(T_P)\right) = \mathbb{E}(I_C) \approx \frac{1}{N}\sum_{i=1}^{N} I_C(\tilde{\boldsymbol{x}}_i) \tag{41}$$

in which $\tilde{\boldsymbol{x}}_i$ is one out of N independent and identically distributed drawn samples from the joint density $p(\boldsymbol{x}_{E,k:k+T_P}, \boldsymbol{x}_{V_i,k:k+T_P})$ and the unbiased estimate converging almost surely to the true collision probability by the strong law of large numbers with convergence rate of order $\mathcal{O}(1/\sqrt{N})$

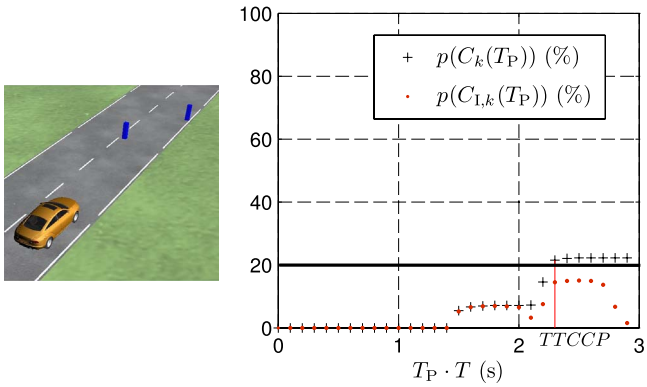

Fig. 11. We consider a vehicle moving with constant velocity on a lane with two obstacles (blue) standing left and right in a way that the vehicle can just get through by moving straight. The obstacles have a longitudinal offset slightly larger than the vehicle length. We first have a look at the collision probabilities at future time *instants*, $p(C_{I,k}(T_P))$, which are shown in red for a prediction horizon of 3 s. Two plateaus are clearly visible, which stem from predicted collisions with the two obstacles under consideration of vehicle and obstacle extensions. The plateau from the obstacle further away is higher due to the larger variance of the predicted position at greater prediction times. This results in a larger amount of predicted vehicle configurations overlapping with the obstacle. For predicted time instants in-between the plateaus ($T_P \cdot T \approx 2.1$ s), the collision probability decreases as the predicted location is now mostly right between the longitudinal positions of both obstacles and thus no collision occurs. In every predicted time step, $p(C_{I,k}(T_P))$ is lower than the CCP fixed at 20%. Note that the maximal probability over time *instants* would be the same if either only one or both obstacles were present (due to the fact that simultaneous collisions with both obstacles at a single future time step are impossible in this scenario), which contradicts intuition. In contrast, we now have a look at the collision probability over a future time *span*, $p(C_k(T_P))$, shown in black. Its shape is similar to $p(C_{I,k}(T_P))$ at first but does not decrease as all trajectories that have already collided at least once with the first obstacle are still considered. For longer prediction time horizons, the second obstacle now raises the probability $p(C_k(T_P))$ above CCP and the situation is regarded as critical with a TTCCP of 2.3 s.

[42]. Each sample thus corresponds to two complete predicted trajectories. Although, following (24), the trajectories of the different vehicles can be drawn independently of each other, the specification of the Monte Carlo estimate in this more general form is advantageous as it then becomes directly obvious that only a single summation over simultaneously drawn samples from both individual distributions, $p(\boldsymbol{x}_{E,k:k+T_P})$ and $p(\boldsymbol{x}_{V_i,k:k+T_P})$, is required. This is further elaborated and justified in [35]. This way, much fewer samples are needed to obtain the same estimation error in opposition to a naive double

$$p(C_k(T_P)) = \int_{\boldsymbol{x}_{\mathrm{PFS},k}} \overbrace{\underbrace{\left(\int_{\boldsymbol{x}_{V_f,k+T_P}} \cdots \int_{\boldsymbol{x}_{V_1,k+T_P}} \int_{\boldsymbol{x}_{E,k+T_P}}\right) \cdots \left(\int_{\boldsymbol{x}_{V_f,k}} \cdots \int_{\boldsymbol{x}_{V_1,k}} \int_{\boldsymbol{x}_{E,k}}\right)}_{(T_P+1)\cdot(f+1)} I_{C_\mathrm{g}}(\boldsymbol{x}_{E,k:k+T_P}, \boldsymbol{x}_{V_1,k:k+T_P}, \ldots, \boldsymbol{x}_{V_f,k:k+T_P}, \boldsymbol{x}_{\mathrm{PFS},k})}^{f+1}$$
$$p(\boldsymbol{x}_{E,k:k+T_P}, \boldsymbol{x}_{V_1,k:k+T_P}, \ldots, \boldsymbol{x}_{V_f,k:k+T_P}, \boldsymbol{x}_{\mathrm{PFS},k}) (d\boldsymbol{x}_{E,k} d\boldsymbol{x}_{V_1,k} \ldots d\boldsymbol{x}_{V_f,k}) \ldots (d\boldsymbol{x}_{E,k+T_P} d\boldsymbol{x}_{V_1,k+T_P} \ldots d\boldsymbol{x}_{V_f,k+T_P}) d\boldsymbol{x}_{\mathrm{PFS},k}$$

with the general indicator function

$$I_{C_\mathrm{g}}(\boldsymbol{x}_{E,k:k+T_P}, \boldsymbol{x}_{V_1,k:k+T_P}, \ldots, \boldsymbol{x}_{V_f,k:k+T_P}, \boldsymbol{x}_{\mathrm{PFS},k}) = \begin{cases} 1, \exists m \in \{k{:}k+T_P\}\colon \mathcal{S}(\boldsymbol{x}_{E,m}) \bigcap \left(\bigcup_{i=1}^{f} \mathcal{S}(\boldsymbol{x}_{V_i,m}) \bigcup \mathcal{S}(\boldsymbol{x}_{\mathrm{PFS},k})\right) \neq \emptyset \\ 0, \text{else} \end{cases} \tag{39}$$

TABLE II
SIMULATION PARAMETERS

	Parameter	Value
FR	$3\sigma_{\Delta a_{\mathrm{R,lon}}}; 3\sigma_{y_\mathrm{R}}; T_\mathrm{c}; u; 3\sigma_{\psi_\mathrm{R}}$	$0.2\,\mathrm{m/s^2}; \frac{1}{2}(w_\mathrm{L}-w_\mathrm{V}); 1.5\,\mathrm{s}; \frac{1}{2}w_\mathrm{L}; 5^\circ$
FV	$\tau_\mathrm{r}; a_{\mathrm{f,min}}; a_{\mathrm{f,max}}; 3\sigma_{\Delta a_{\mathrm{R,lon}}}; 3\sigma_{y_\mathrm{R}}; T_\mathrm{c}; u; 3\sigma_{\psi_\mathrm{R}}$	$2\,\mathrm{s}; -3.5\,\mathrm{m/s^2}; 2.5\,\mathrm{m/s^2}; 0.2\,\mathrm{m/s^2}; \frac{1}{2}(w_\mathrm{L}-w_\mathrm{V}); 1.5\,\mathrm{s}; \frac{1}{2}w_\mathrm{L}; 5^\circ$
TB	$d_\mathrm{r}; a_{\mathrm{min}}; 3\sigma_{y_\mathrm{R}}; T_\mathrm{c}; u; 3\sigma_{\psi_\mathrm{R}}$	$1\,\mathrm{m}; -8\,\mathrm{m/s^2}; \frac{1}{2}(w_\mathrm{L}-w_\mathrm{V}); 1.5\,\mathrm{s}; \frac{1}{2}w_\mathrm{L}; 5^\circ$
LC	$3\sigma_{\Delta a_{\mathrm{R,lon}}}; 3\sigma_{y_{\mathrm{R,s}}}$	$0.2\,\mathrm{m/s^2}; \frac{1}{2}(w_\mathrm{L}-w_\mathrm{V})$
TU	$a_{\mathrm{min}}; a_{\mathrm{c,max}}; 3\sigma_{\Delta a_{\mathrm{R,lon}}}; 3\sigma_{y_\mathrm{R}}; T_\mathrm{c}; u; 3\sigma_{\psi_\mathrm{R}}$	$-8\,\mathrm{m/s^2}; 4\,\mathrm{m/s^2}; 0.2\,\mathrm{m/s^2}; \frac{1}{2}(w_\mathrm{L}-w_\mathrm{V}); 1.5\,\mathrm{s}; \frac{1}{2}w_\mathrm{L}; 5^\circ$
TR	$3\sigma_{\Delta a}; 3\sigma_{\Delta\omega}$	$0.2\,\mathrm{m/s^2}; 1.5\,^\circ/\mathrm{s}$
PFS	$N_\mathrm{b}; d$	$70; 3$
—	$w_\mathrm{L}; w_\mathrm{V}; T; N;$ CCP	$3.5\,\mathrm{m}; 1.5\,\mathrm{m}; 0.1\,\mathrm{s}; 5000; 0.2$

summation over individual trajectory samples. Another performance gain is achieved by realizing that samples drawn from $p(\boldsymbol{x}_{E,k:k+T_P})$ for the ego vehicle can be reused in evaluating (22) for the different vehicles and in (31) for the collision probability with the static environment due to the mentioned independence assumption between vehicle trajectories. Moreover, trajectory samples do not have to be generated for the whole prediction horizon $\{k{:}k+T_P\}$ but only until the first collision is detected as the combined collision event probability (intentionally) does not change in the case of subsequent collisions. All in all, the run-time for the criticality assessment scales linearly with the number of dynamic objects and is—due to the PFS map approach—nearly independent of the complexity of the static environment.

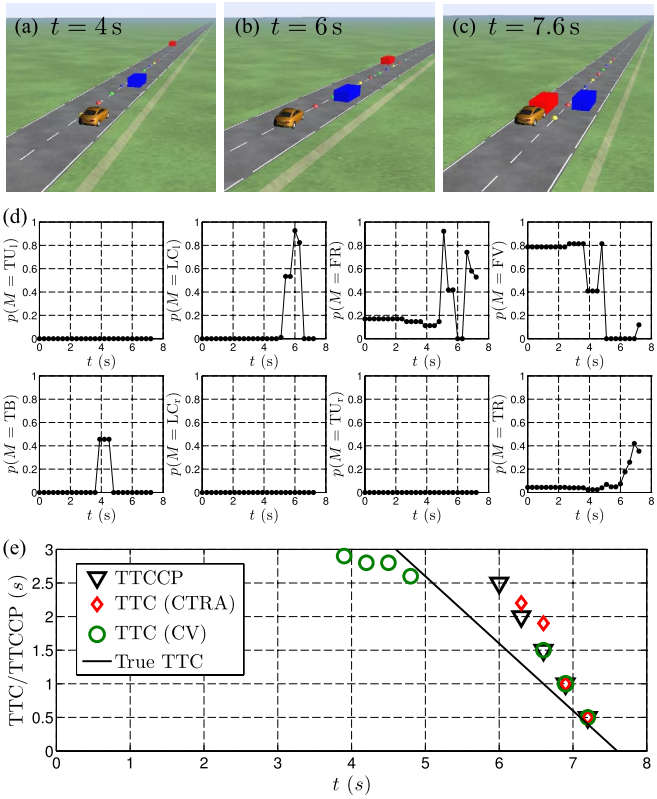

Fig. 12. Lane change scenario and collision with oncoming vehicle. Traffic scene (a), (b), (c); maneuver probabilities (d); TTC/TTCCP evolution (e).

IV. IMPLEMENTATION AND RESULTS

The complete system has been implemented in C++ and coupled with the simulation environment IPG Carmaker. For Bayesian network inference, we employ the junction tree algorithm [43], which provides exact and fast inference results for discrete random variables as used in our case. Simulation parameters are summarized in Table II. In the following, three exemplary driving scenarios are shown to illustrate the capabilities and scope of the system.

In the first example visualized in Fig. 12(a)–(c), the ego vehicle (orange) approaches another vehicle (blue) driving in the same direction on the same lane, decelerates rapidly ($t \approx 4$ s) to successfully prevent a collision, and subsequently performs a lane change ($t \approx 6$ s) to the left to overtake. On the adjacent lane, however, an oncoming vehicle (red) approaches with which the ego vehicle finally collides at $t = 7.6$ s. The maneuver estimation (Fig. 12(d)) clearly shows the individual driving maneuvers (in successive order: FV, TB, LC_l, FR) for the ego vehicle—the other two vehicles just follow the road with constant velocity. The derived criticality metrics TTC (CV/CTRA) and TTCCP are shown in Fig. 12(e). The TTC calculated via a CV model generates false positive criticality values at $t \approx 4$ s as it does not consider the deceleration of the ego vehicle before performing the lane change. The CTRA-based TTC and our approach do not show this undesirable result. Our approach, at this stage, mainly predicts via TB and—to a lesser extend—via a FV model. Additionally, we see that the true collision can be detected first by our method due to mainly predicting via a LC model during the lane change. Note that the first two TTC (CTRA) values stem from another false collision detection of the ego vehicle with the blue vehicle on the same lane as the predicted trajectories with high turn rate cross the original road again—a clearly non-reasonable prediction. With this in mind, our system is able to generate the criticality metric 0.9 s earlier than the CTRA model and 0.6 s earlier than a CV model. This allows timelier driver warnings—1.6 s before the imminent collision in this scenario. Note that the true TTC progression is impossible to match for any prediction method here as, for example, 3 s in advance (at $t = 4.6$ s), absolutely no evidence is available that would imply an impending lane change. Our approach, however, clearly converges to the true collision time $t = 7.6$ s, the closer we reach this point in time. The deviations between TTCCP and true TTC before the collision event stem from a difference between the lane change prediction model and the true, executed lane change trajectory.

The second scenario is visualized in Fig. 13(a)–(c). The ego vehicle (orange) approaches an intersection while another crossing vehicle (red) approaches from the left. The ego vehicle turns to the left and finally collides with constant velocity with a standing obstacle. We first notice in Fig. 13(e) that the TTC for both the deterministic CTRA and the CV model do not provide any indication of the dangerous intersection approach although every minor acceleration change could lead to a collision. The TTCCP value, in contrast, clearly indicates the danger several seconds (3 s) in advance by predicting both vehicles (mainly) according to a FR model in which the future acceleration

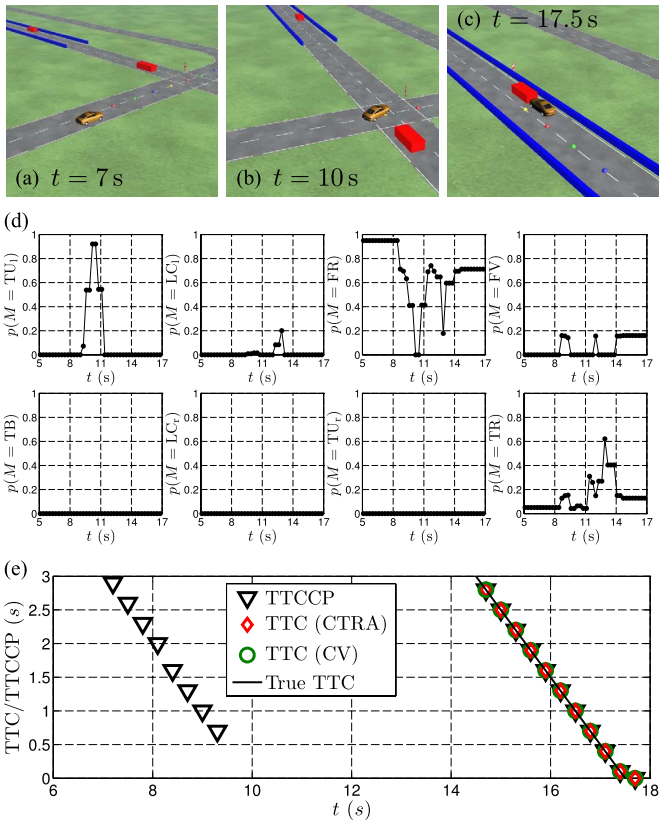

Fig. 13. Turning scenario (a) with near-collision with cross-traffic (b) and subsequent collision with stationary vehicle (c). Maneuver probabilities (d); TTC/TTCCP evolution (e).

realizations are considered uncertain. Eventual alarms triggered by the low TTCCP values at $t \approx 9$ s should not be considered false alarms as all available knowledge at this point in time implies a critical situation that is only resolved when the situation evolves further. As soon as it becomes evident that probably no collision occurs, the TTCCP vanishes (rises to ∞) at $t = 9.6$ s. The ego vehicle then performs the turn to the left at $t \approx 10$ s, which is correctly identified via the Bayesian network, before it again follows the road, see Fig. 13(d). The peak within the trash maneuver class after the turning stems from the vehicle motion further to the right than necessary to follow the road, so that this could also mean that the driver accidentally leaves the road. After the turning, the ego vehicle approaches the standing obstacle with constant velocity and collides at $t = 17.5$ s. In this unambiguous case, the TTCCP reasonably coincides with the TTC.

The third scenario, visualized in Fig. 14(a)–(c), is devoted to the advantages of the trash maneuver class and the incorporation of PFS maps for criticality assessment. At first, the ego vehicle (orange) follows the road flawlessly. At $t \approx 2.7$ s, however, it deviates from the straight road course to the right, e.g. due to driver inattentiveness, and is near a collision with the right guardrail. Before colliding, the vehicle gets back on track and starts executing a lane change to the left shortly afterwards ($t \approx 7$ s). This lane change is, however, not completed but aborted halfway through at $t \approx 10$ s, and the vehicle moves in-between both lanes for the rest of the scenario. At $t \approx 15$ s, it reaches a narrowing of the road, e.g. a construction side,

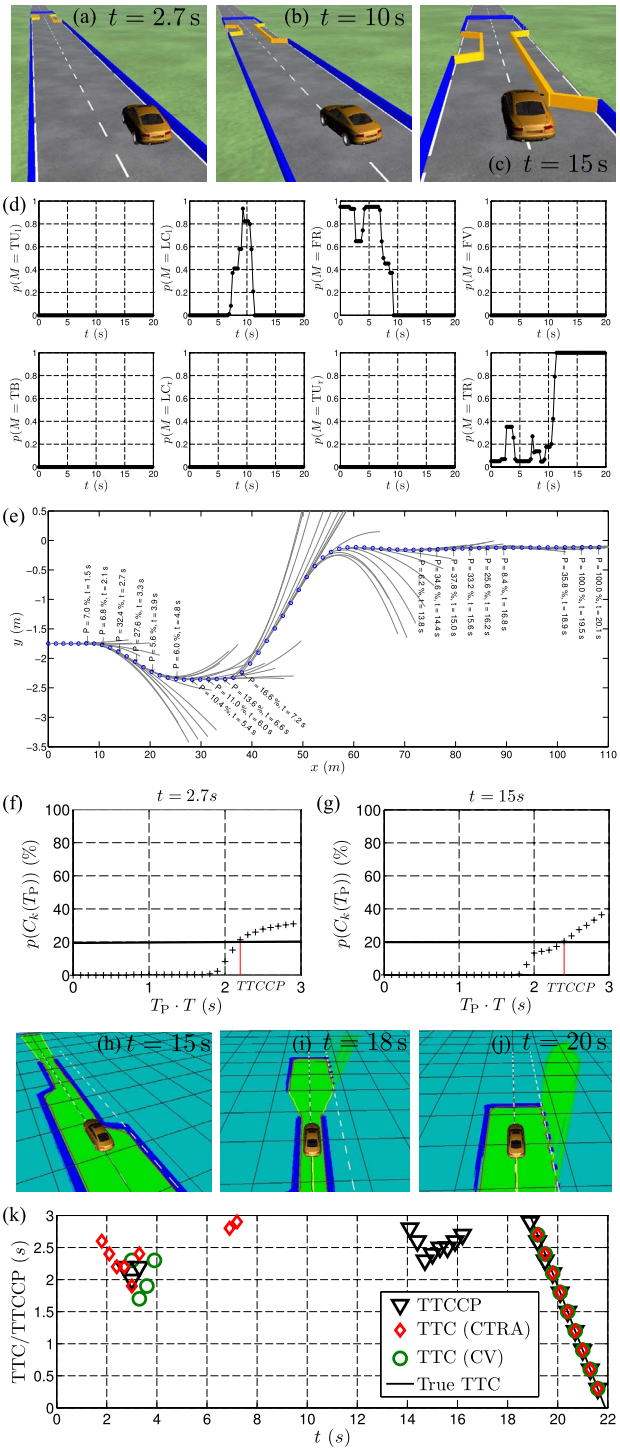

Fig. 14. Accidental deviation from road course with near-collision (a), followed by a lane change to the left, which is aborted halfway through (b), and subsequent drive through a narrowing with final collision with road blocking (c). Maneuver probabilities (d); bird's eye view with corresponding combined collision probability for 3 s prediction horizon (e); combined collision probabilities over prediction horizon length (f), (g); PFS maps overlaid corresponding occupancy grid maps (h), (i), (j); TTC/TTCCP evolution (k).

which gets even more pronounced as soon as also the left lane becomes partially blocked, see Fig. 14(c). Finally, the vehicle inevitably collides with the road block at $t = 21.9$ s. At the beginning, the ego vehicle motion along the road is explained by the FR model as shown in Fig. 14(d). As soon as the vehicle departs from the road course to the right, the motion cannot

be reasonably explained by the standard maneuver classes any more. As a consequence, the maneuver detection shows a rise in the trash maneuver class probability to nearly 40% and the abnormal situation becomes evident. Without the trash class, the system would distribute the probability mass between the standard maneuvers, which is clearly inappropriate in this situation and would prevent the detection of this critical situation. Note that because the deviation from the road is not extreme, there is still a relatively high probability of a FR maneuver during this time, which rises back to the high initial value as soon as the driver avoids the collision with the right guardrail and gets back on track at $t \approx 5$ s. The subsequent start of the LC maneuver is then clearly recognized similarly to the first scenario, but as soon as the driver aborts the lane change at $t \approx 10$ s and drives in-between both lanes, the trash class probability rises rapidly and remains high for the rest of the scenario. This is a reasonable inference result as no standard maneuver corresponds to this driver action. Fig. 14(e) additionally shows the bird's eye view of the vehicle position along with the mean predicted CTRA trajectories of the trash maneuver class and the corresponding combined collision probabilities over the respective 3 s prediction horizon. As long as the driver follows the road at the beginning, the criticality remains near zero due to the bounded variance of the lateral coordinate's Ornstein-Uhlenbeck model so that only a negligible number of predicted trajectories collide with the guardrail. This advantageous property eliminates false warnings in this standard situation. As soon as the vehicle deviates to the right, however, the collision probability rises due to the trash maneuver class's CTRA model predictions, which allows driver warnings or interventions. For better insight, Fig. 14(f) additionally visualizes the combined collision probability as a function of the prediction length at that time ($t = 2.7$ s). The consistent rise in collision probability over the prediction horizon exceeds the CCP of 20% at TTCCP $= 2.2$ s in the future, which is also reflected in the TTCCP evolution in Fig. 14(k). The TTCCP around this time is, in value, similar to the deterministic TTC (CTRA) but emerges slightly afterwards because the trash maneuver probability has to build up first. Note that the TTC (CV) values are delayed in comparison to TTC (CTRA) and TTCCP as no turn rates are considered. Therefore, both the rising criticality and the subsequent collision avoidance by the driver's countersteer are reflected too late in the TTC (CV). At the subsequent start of the lane change, the TTC (CTRA) generates false values at $t \approx 7$ s as the CTRA predictions collide with the left guardrail due to the strong yaw rate at the beginning of the lane change. These false criticality values are suppressed by our approach due the predominant prediction via the LC model at this time. Between $t \approx 15$ s and $t \approx 18$ s, the vehicle drives through the already mentioned road narrowing. The PFS maps overlaid their corresponding occupancy grid maps (occupied shown in blue, free in green) are depicted in Fig. 14(h) and (i) for these times. The narrowing is clearly visible in the map representations. The situation is considered critical as any minor steering would result in a collision. The TTCCP can represent this criticality, whereas the TTC does not exist. A closer look at the collision probability evolution at $t = 15$ s in Fig. 14(g) reveals a first increase of $p(C_k(T_P))$ approximately 1.8 s in the future, followed by a plateau and a further increase after 2.3 s prediction time. This evolution is the result of the two subsequent narrowings, first only on the right, later also on the left. It becomes obvious that the first narrowing does not suffice to exceed the CCP but only the second one provokes a situation criticality high enough to generate a TTCCP value of 2.4 s. This result is in accordance with human reasoning in this situation, see Fig. 14(c). Note that the TTCCP values remain approximately constant during the narrow road passage because the criticality does not change as long as there is no steering against the boundary. At the end of the narrowing, the TTCCP disappears (rises to ∞) before finally converging towards the true collision time with the road block at $t = 21.9$ s, which is apparent also in the PFS map in Fig. 14(j). The combined collision probability rises to 100% here, as all trash maneuver class's trajectories collide with the outer B-spline curve at the end of the scenario due to the completely blocked road without any driver reaction.

V. Conclusion

The article presented an integrated approach to long-term trajectory prediction and criticality assessment, which considers not only maneuver and motion uncertainties of all vehicles but also arbitrary static environments with the help of PFS maps. A Bayesian maneuver detection combined with maneuver-specific, uncertain trajectory predictions is used to calculate the introduced criticality time metric TTCCP as a generalization of TTC. The system suppresses false warnings, generates timelier true warnings in comparison to TTC, and allows the generation of warnings in critical almost-collision situations, in which the TTC does not even exist. An additional trash maneuver class permits the detection of abnormal events that do not correspond to standard driving maneuvers. Although the approach contains novelties in the areas of maneuver detection, trajectory prediction, and criticality assessment, the main contribution might lie in the throughout design considerations of the individual components with the aim of long-term criticality assessment in mind.

Acknowledgment

We kindly thank the Continental AG for their great cooperation within the PRORETA 3 project [44], which aimed at the development of future concepts for integrated driver assistance systems. We further thank Igor Achieser, Yuanwen Qin, Julien Seitz, and Gerrit Wege for the numerous fruitful discussions and their help in implementing the concept.

References

[1] M. Schreier, V. Willert, and J. Adamy, "Bayesian, maneuver-based, long-term trajectory prediction and criticality assessment for driver assistance systems," in *Proc. IEEE Int. Conf. Intell. Transp. Syst.*, Qingdao, China, Oct. 2014, pp. 334–341.

[2] C. Hermes, C. Wöhler, K. Schenk, and F. Kummert, "Long-term vehicle motion prediction," in *Proc. IEEE Intell. Veh. Symp.*, Xi'an, China, Jun. 2009, pp. 652–657.

[3] D. Vasquez, T. Fraichard, and C. Laugier, "Incremental learning of statistical motion patterns with growing hidden Markov models," *IEEE Trans. Intell. Transp. Syst.*, vol. 10, no. 3, pp. 403–416, Sep. 2009.

[4] M. Althoff, O. Stursberg, and M. Buss, "Model-based probabilistic collision detection in autonomous driving," *IEEE Trans. Intell. Transp. Syst.*, vol. 10, no. 2, pp. 299–310, Jun. 2009.
[5] A. Broadhurst, S. Baker, and T. Kanade, "Monte Carlo road safety reasoning," in *Proc. IEEE Intell. Veh. Symp.*, Las Vegas, NV, USA, Jun. 2005, pp. 319–324.
[6] A. Eidehall and L. Petersson, "Statistical thread assessment for general road scenes using Monte Carlo sampling," *IEEE Trans. Intell. Transp. Syst.*, vol. 9, no. 1, pp. 137–147, Mar. 2008.
[7] A. Lawitzky *et al.*, "Interactive scene prediction for automotive applications," in *Proc. IEEE Intell. Veh. Symp.*, Gold Coast, Qld., Australia, Jun. 2013, pp. 1028–1033.
[8] T. Gindele, R. Brechtel, and R. Dillmann, "A probabilistic model for estimating driver behaviors and vehicle trajectories in traffic environments," in *Proc. IEEE Int. Conf. Intell. Transp. Syst.*, Madeira Island, Portugal, Sep. 2010, pp. 1625–1631.
[9] J. Sörstedt, L. Svensson, F. Sandblom, and L. Hammarstrand, "A new vehicle motion model for improved predictions and situations assessment," *IEEE Trans. Intell. Transp. Syst.*, vol. 12, no. 4, pp. 1209–1219, Dec. 2011.
[10] C. Schlenoff, R. Madhavan, and Z. Kootbally, "PRIDE: A hierarchical, integrated prediction framework for autonomous on-road driving," in *Proc. IEEE Int. Conf. Robot. Autom.*, Orlando, FL, USA, May 2006, pp. 2348–2353.
[11] T. Hülnhagen *et al.*, "Maneuver recognition using probabilistic finite-state machines and fuzzy logic," in *Proc. IEEE Intell. Veh. Symp.*, San Diego, CA, USA, Jun. 2010, pp. 65–70.
[12] J. Schneider, A. Wilde, and K. Naab, "Probabilistic approach for modeling and identifying driving situations," in *Proc. IEEE Intell. Veh. Symp.*, Eindhoven, The Netherlands, Jun. 2008, pp. 343–348.
[13] R. Schubert, K. Schulze, and G. Wanielik, "Situation assessment for automatic lane-change maneuvers," *IEEE Trans. Intell. Transp. Syst.*, vol. 11, no. 3, pp. 607–616, Sep. 2010.
[14] D. Kasper *et al.*, "Object-oriented Bayesian network for detection of lane change maneuvers," *IEEE Intell. Transp. Syst. Mag.*, vol. 4, no. 1, pp. 1–10, Jan. 2012.
[15] S. Klingelschmitt, M. Platho, H.-M. Groß, V. Willert, and J. Eggert, "Combining behavior and situation information for reliably estimating multiple intentions," in *Proc. IEEE Intell. Veh. Symp.*, Dearborn, MI, USA, Jun. 2014, pp. 388–393.
[16] M. Platho, H.-M. Groß, and J. Eggert, "Learning driving situations and behavior models from data," in *Proc. IEEE Int. Conf. Intell. Transp. Syst.*, The Hague, The Netherlands, Oct. 2013, pp. 276–281.
[17] I. Dagli, M. Brost, and G. Breuel, "Action recognition and prediction for driver assistance systems using dynamic belief networks," *Lecture Notes Comput. Sci.*, vol. 2592, pp. 179–194, 2003.
[18] H. Berndt and K. Dietmayer, "Driver intention inference with vehicle onboard sensors," in *Proc. IEEE Int. Conf. Veh. Electron. Safety*, Pune, India, Nov. 2009, pp. 102–107.
[19] M. Tsogas, X. Dai, G. Thomaidis, P. Lytrivis, and A. Amditis, "Detection of maneuvers using evidence theory," in *Proc. IEEE Intell. Veh. Symp.*, Eindhoven, The Netherlands, Jun. 2008, pp. 126–131.
[20] M. Hülsen, J. M. Zöllner, and C. Weiss, "Traffic intersection situation description ontology for advanced driver assistance," in *Proc. IEEE Intell. Veh. Symp.*, Baden-Baden, Germany, Jun. 2011, pp. 993–999.
[21] E. Käfer, C. Hermes, C. Wöhler, H. Ritter, and F. Kummert, "Recognition of situation classes at road intersections," in *Proc. IEEE Int. Conf. Robot. Autom.*, Anchorage, AK, USA, May 2010, pp. 3960–3965.
[22] S. Bonnin *et al.*, "General behavior prediction by a combination of scenario-specific models," *IEEE Trans. Intell. Transp. Syst.*, vol. 15, no. 4, pp. 1478–1488, Aug. 2014.
[23] C. Laugier *et al.*, "Probabilistic analysis of dynamic scenes and collision risks assessment to improve driving safety," *IEEE Intell. Transp. Syst. Mag.*, vol. 3, no. 4, pp. 4–19, Winter 2011.
[24] J. Hillenbrand, A. M. Spieker, and K. Kroschel, "A multilevel collision mitigation approach—Its situation assessment, decision making, and performance tradeoffs," *IEEE Trans. Intell. Transp. Syst.*, vol. 7, no. 4, pp. 528–540, Dec. 2006.
[25] A. Tamke, T. Dang, and G. Breuel, "A flexible method for criticality assessment in driver assistance systems," in *Proc. IEEE Intell. Veh. Symp.*, Baden-Baden, Germany, Jun. 2011, pp. 697–702.
[26] A. Berthelot, A. Tamke, T. Dang, and G. Breuel, "Stochastic situation assessment in advanced driver assistance system for complex multi-objects traffic situations," in *Proc. IEEE Int. Conf. Intell. Robot. Syst.*, Vilamoura, Portugal, Oct. 2012, pp. 1180–1185.
[27] A. Houénou, P. Bonnifait, and V. Cherfaoui, "Risk assessment for collision avoidance systems," in *Proc. IEEE Int. Conf. Intell. Transp. Syst.*, Qingdao, China, Oct. 2014, pp. 386–391.
[28] J. Eggert, "Predictive risk estimation for intelligent ADAS functions," in *Proc. IEEE Int. Conf. Intell. Transp. Syst.*, Qingdao, China, Oct. 2014, pp. 711–718.
[29] S. Lefèvre, C. Laugier, and J. Ibañez-Guzmán, "Risk assessment at road intersections: Comparing intention and expectation," in *Proc. IEEE Intell. Veh. Symp.*, Alcalá de Henares, Spain, Jun. 2012, pp. 165–171.
[30] J. Pearl, *Probabilistic Reasoning in Intelligent Systems: Networks of Plausible Inference*, 2nd ed. San Francisco, CA, USA: Morgan Kaufmann, 1988.
[31] K. Schmitt and R. Isermann, "Vehicle state estimation in curved road coordinates for a driver assistance system for overtaking situations," in *Proc. Int. Symp. Dyn. Veh. Roads Tracks*, Stockholm, Sweden, Aug. 2009, pp. 1–12.
[32] W. Yao, H. Zhao, P. Bonnifait, and H. Zha, "Lane change trajectory prediction by using recorded human driving data," in *Proc. IEEE Intell. Veh. Symp.*, Gold Coast, Qld., Australia, Jun. 2013, pp. 430–436.
[33] Y. Bar-Shalom, X.-R. Li, and T. Kirubarajan, *Estimation With Applications to Tracking and Navigation. Theory, Algorithms and Software*. New York, NY, USA: Wiley-Interscience, 2001.
[34] H. Winner, B. Danner, and J. Steinle, "Adaptive cruise control," in *Handbuch Fahrerassistenzsysteme*, 2nd ed. Wiesbaden, Germany: Vieweg+Teubner, 2012, ch. 32, pp. 478–521.
[35] N. E. Du Toit and J. W. Burdich, "Probabilistic collision checking with chance constraints," *IEEE Trans. Robot.*, vol. 27, no. 4, pp. 809–815, Aug. 2011.
[36] M. Schreier and V. Willert, "Robust free space detection in occupancy grid maps by methods of image analysis and dynamic B-spline contour tracking," in *Proc. IEEE Int. Conf. Intell. Transp. Syst.*, Anchorage, AK, USA, Sep. 2012, pp. 514–521.
[37] M. Schreier, V. Willert, and J. Adamy, "From grid maps to parametric free space maps—A highly compact, generic environment representation for ADAS," in *Proc. IEEE Intell. Veh. Symp.*, Gold Coast, Qld., Australia, Jun. 2013, pp. 938–944.
[38] M. Schreier, "Bayesian environment representation, prediction, and criticality assessment for driver assistance systems," Ph.D. dissertation, TU Darmstadt, Darmstadt, Germany, 2016.
[39] M. Schreier, V. Willert, and J. Adamy, "Grid mapping in dynamic road environments: Classification of dynamic cell hypothesis via tracking," in *Proc. IEEE Int. Conf. Robot. Autom.*, Hong Kong, China, Jun. 2014, pp. 3995–4002.
[40] M. Schreier, V. Willert, and J. Adamy, "Compact representation of dynamic driving environments for ADAS by parametric free space and dynamic object maps," *IEEE Trans. Intell. Transp. Syst.*, vol. 17, no. 2, pp. 367–384, Feb. 2016.
[41] C. de Boor, "A practical guide to splines," in *Applied Mathematical Sciences*, vol. 27. New York, NY, USA: Springer-Verlag, 1978.
[42] J. M. Hammersley and D. C. Handscomb, *Monte Carlo Methods*, M. S. Bartlett, Ed. London, U.K.: Methuen & Co. Ltd., 1964.
[43] S. L. Lauritzen and D. J. Spiegelhalter, "Local computations with probabilities on graphical structures and their application to expert systems," *J. Roy. Statist. Soc. B, Methodol.*, vol. 50, no. 2, pp. 157–224, 1988.
[44] H. Winner *et al.*, "PRORETA 3: Comprehensive driver assistance by safety corridor and cooperative automation," in *Handbook of Driver Assistance Systems. Basic Information, Components and Systems for Active Safety and Comfort*, Switzerland: Springer-Verlag, 2016, ch. 58, pp. 1449–1469.

Matthias Schreier received the M.Sc. degree (with distinction) in mechatronics from Leibniz Universität Hannover, Hannover, Germany, in 2010, with a focus on system dynamics and control as well as robotics. He is currently working toward the Dr.-Ing. degree in the area of advanced driver assistance systems with the Control Methods and Robotics Laboratory, Technical University of Darmstadt, Darmstadt, Germany.

His main research interests are in the field of compact and robust environment representations for intelligent vehicles, as well as in the prediction of dangerous traffic situations. Within the development of the driver assistance system PRORETA 3, he has been responsible for the environment representation and prediction.

Mr. Schreier has served as a reviewer for *IEEE Intelligent Transportation Systems Magazine*, IEEE Intelligent Transportation Systems Conferences, and IEEE Intelligent Vehicles Symposium. He was a recipient of a scholarship and the Dr.-Jürgen-Ulderup Award 2012 for outstanding student results, as well as a Best Paper Finalist Award at the 2012 IEEE International Conference on Mechatronics and Automation.

Volker Willert received the Dipl.-Ing. degree in electrical engineering and information technology and the Dr.-Ing. degree in control theory and robotics, with a focus on dynamical computer vision, from Technical University of Darmstadt (TU Darmstadt), Darmstadt, Germany, in 2002 and 2006, respectively.

From 2005 to 2009, he was a Senior Scientist at Honda Research Institute Europe GmbH. Since July 2009, he has been with the Chair of the Control Methods and Robotics Laboratory, TU Darmstadt, and heads the research group Machine Vision and Mobile Robotics. His main research interests are in the fields of machine intelligence, computer vision, distributed controls, and machine learning for mobile robotics, multiagent systems, and driver assistance systems.

Dr.-Ing. Willert is an Akademischer Oberrat and a Lecturer. He has served as a reviewer for numerous IEEE conferences and journals. He was a recipient of the main Best Paper Award at the IEEE International Conference on Machine Learning and Applications 2007, as well as the Best Paper Award at the 2009 IEEE International Conference on Computer Vision, Workshop Dynamical Vision.

Jürgen Adamy received the Diploma and Dr.-Ing. degrees in electrical engineering from Technical University of Dortmund, Dortmund, Germany, in 1987 and 1991, respectively.

Then, he was an Engineer and a Manager in the area of control applications at Siemens, Erlangen, Germany. In 1998, he became a Full Professor at Technical University of Darmstadt, Darmstadt, Germany, where he is the Head of the Control Methods and Robotics Laboratory and currently the Director of the Institute of Automatic Control and Mechatronics and Dean of the Department of Electrical Engineering and Information Technology. His research interests are in the areas of nonlinear control, fuzzy systems, and mobile robots.